REPORT DOCUMENTATION PAGE

Form Approved OMB NO. 0704-0188

1. REPORT DATE (DD-MM-YYYY)	2. REPORT TYPE	3. DATES COVERED (From - To)
23-12-2009	Final Report	1-Jul-2006 - 30-Sep-2009

4. TITLE AND SUBTITLE

Hybrid R-Fe-B/R-Co Magnets with Improved Thermal Stability

5a. CONTRACT NUMBER

W911NF-06-1-0274

5b. GRANT NUMBER

5c. PROGRAM ELEMENT NUMBER

611102

6. AUTHORS

Y. Shen, A. Higgins, C. Chen, and S. Liu

5d. PROJECT NUMBER

5e. TASK NUMBER

5f. WORK UNIT NUMBER

7. PERFORMING ORGANIZATION NAMES AND ADDRESSES

University of Dayton
Office of Contracts & Grants
University of Dayton
Dayton, OH 45469 -0104

8. PERFORMING ORGANIZATION REPORT NUMBER

9. SPONSORING/MONITORING AGENCY NAME(S) AND ADDRESS(ES)

U.S. Army Research Office
P.O. Box 12211
Research Triangle Park, NC 27709-2211

10. SPONSOR/MONITOR'S ACRONYM(S)

ARO

11. SPONSOR/MONITOR'S REPORT NUMBER(S)

49631-MS.1

12. DISTRIBUTION AVAILIBILITY STATEMENT

Approved for Public Release; Distribution Unlimited

13. SUPPLEMENTARY NOTES

The views, opinions and/or findings contained in this report are those of the author(s) and should not contrued as an official Department of the Army position, policy or decision, unless so designated by other documentation.

14. ABSTRACT

Permanent magnets combining high magnetic performance and good thermal stability are needed in various US Army applications. Hybrid Pr2(Fe,Co)14B /Pr(Co,Fe)5 magnets were studied and synthesized. The possibility of applying nanoparticles to synthesize bulk magnets was also explored.

The magnetic property of (BH)max = 36.9 MGOe was obtained in a hybrid Pr14.1Fe73.3Co5.1Ga0.5B7.1/Pr(Co0.8Fe0.2)5 magnet . Hybrid Pr2(Fe,Co)14B/ Pr(Co,Fe)5 magnets

15. SUBJECT TERMS

permanent magnets, Nd-Fe-B, Sm2Co17, Pr-Fe-B, PrCo5, thermal stability, nanograin structure, nanoparticles

16. SECURITY CLASSIFICATION OF:			17. LIMITATION OF ABSTRACT	15. NUMBER OF PAGES	19a. NAME OF RESPONSIBLE PERSON
a. REPORT	b. ABSTRACT	c. THIS PAGE			Shiqiang Liu
UU	UU	UU	UU		19b. TELEPHONE NUMBER: 937-229-3272

UDR-TR-2009-00204

HYBRID R-Fe-B/R-Co MAGNETS WITH IMPROVED THERMAL STABILITY

December 2009

Final Progress Report for
Contract No. W911NF-06-1-0274

For Period

July 2006 through September 2009

Prepared for:

US Army ARO
PO Box 12211
Research Triangle Park, NC 27709-2211

Prepared by:

Y. Shen, A. Higgins, C. Chen, and S. Liu
University of Dayton Research Institute
Metals and Ceramics Division
300 College Park
Dayton, Ohio 45469-0174

REPORT DOCUMENTATION PAGE

Form Approved
OMB No. 0704-0188

1. REPORT DATE *(DD-MM-YYYY)*	**2. REPORT TYPE**	**3. DATES COVERED** *(From - To)*
21 December 2009	Final Report	July 2006 – September 2009

4. TITLE AND SUBTITLE

Hybrid R-Fe-B/R-Co Magnets with Improved Thermal Stability

5a. CONTRACT NUMBER
W911NF-06-1-0274

5b. GRANT NUMBER

5c. PROGRAM ELEMENT NUMBER

6. AUTHOR(S)

Y. Shen, A. Higgins, C. Chen, and S. Liu

5d. PROJECT NUMBER

5e. TASK NUMBER

5f. WORK UNIT NUMBER

7. PERFORMING ORGANIZATION NAME(S) AND ADDRESS(ES)

University of Dayton Research Institute
300 College Park
Dayton, OH 45469-0170

8. PERFORMING ORGANIZATION REPORT NUMBER

UDR-TR-2009-00204

9. SPONSORING / MONITORING AGENCY NAME(S) AND ADDRESS(ES)

US Department of the Army
PO Box 12211
Research Triangle Park, NC 27709-2211

10. SPONSOR/MONITOR'S ACRONYM(S)
US Army ARO

11. SPONSOR/MONITOR'S REPORT NUMBER(S)

12. DISTRIBUTION / AVAILABILITY STATEMENT
Distribution requires prior approval of the sponsor.

13. SUPPLEMENTARY NOTES

14. ABSTRACT

Permanent magnets combining high magnetic performance and good thermal stability are needed in various US Army applications. Hybrid Pr2(Fe,Co)14B/Pr(Co,Fe)5 magnets with nanograin and micrograin structures were studied and synthesized in this project using various processes, including a rapid hot press and hot deformation process, a conventional sintering process, and a rapid induction sintering process. Hybrid $Pr_2(Fe,Co)_{14}B$/ $Pr(Co,Fe)_5$ magnets demonstrated improved long-term thermal stability as compared with those containing no $Pr(Co,Fe)_5$ components. The possibility of applying nanoparticles to synthesize bulk magnets was also explored. A $PrCo_5$ nanopowder was produced by surfactant-assisted high-energy ball milling, and $PrCo_5$ bulk magnets were successfully fabricated by compaction at 200~525°C using the nanopowder. The bulk magnet has cluster microstructure with nanocrystalline. The density of the bulk up to 92% theoretical value was obtained.

15. SUBJECT TERMS

16. SECURITY CLASSIFICATION OF:			**17. LIMITATION OF ABSTRACT**	**18. NUMBER OF PAGES**	**19a. NAME OF RESPONSIBLE PERSON**
a. REPORT	**b. ABSTRACT**	**c. THIS PAGE**			Christina Chen / Sam Liu
Unclassified	Unclassified	Unclassified	SAR	51	**19b. TELEPHONE NUMBER** *(include area code)* 937-229-3454

Standard Form 298 (Rev. 8-98)
Prescribed by ANSI Std. 239.18

TABLE OF CONTENTS

TABLE OF CONTENTS (CONCLUDED)

Section **Page**

LIST OF FIGURES

LIST OF FIGURES (CONTINUED)

LIST OF FIGURES (CONCLUDED)

LIST OF TABLES

ACKNOWLEDGMENTS

The authors are grateful to the US Army Research Office for supporting the work under Contract W911NF-06-1-0274. The authors also would like to express their thanks to Ms. Sheila Liskany of the University of Dayton for her editing of this and previous reports.

ABSTRACT

Permanent magnets combining high magnetic performance and good thermal stability are needed in various US Army applications. Hybrid $Pr_2(Fe,Co)_{14}B/Pr(Co,Fe)_5$ magnets with nanograin and micrograin structures were studied and synthesized in this project using a rapid hot press and hot deformation process, a conventional sintering process, and a rapid induction sintering process. The possibility of applying nanoparticles to synthesize bulk magnets was also explored.

The magnetic property of $(BH)_{max}$ = 36.9 MGOe was obtained in a hybrid $Pr_{14.1}Fe_{73.3}Co_{5.1}Ga_{0.5}B_{7.1}/Pr(Co_{0.8}Fe_{0.2})_5$ magnet containing 10 wt% $Pr(Co,Fe)_5$ component which will give much better thermal stability compared to the commercial available magnets with the same $(BH)_{max}$. In hybrid $Pr_2(Fe,Co)_{14}B/ Pr(Co,Fe)_5$ magnets containing 20 wt% $Pr(Co,Fe)_5$, $(BH)_{max}$ = 33.2 MGOe was obtained. These magnetic properties were obtained in hybrid nanograin magnets prepared using rapid hot press and hot deformation. Hybrid magnets synthesized using the sintering process showed relatively low intrinsic coercivity values. Hybrid $Pr_2(Fe,Co)_{14}B/ Pr(Co,Fe)_5$ magnets demonstrated improved long-term thermal stability as compared with those containing no $Pr(Co,Fe)_5$ components.

In addition, a $PrCo_5$ nanopowder was produced by surfactant-assisted high-energy ball milling. The intrinsic coercivity of the powders milled 4 hours reached 6.7 kOe. Using the nanopowders, $PrCo_5$ bulk magnets were successfully fabricated by compaction at 200~525°C. The bulk magnet has cluster microstructure with nanocrystalline. The density of the bulk up to 92% theoretical value was obtained.

FINAL PROGRESS REPORT

1. BACKGROUND AND PROBLEM STUDIED

It is well known that $Nd_2Fe_{14}B$-based magnets display excellent room temperature magnetic performance with $(BH)_{max}$ up to 50 MGOe. However, their low Curie temperature (312°C) limits the highest operating temperature up to around 100°C and results in poor thermal stability.

On the other hand, Sm_2Co_{17} compound has excellent thermal stability as a result of its very high Curie temperature of 920°C. The commercial $Sm_2(Co,Fe,Cu,Zr)_{17}$ magnets can maintain reliable operation at ~300 to 500°C. Apparently, a wide temperature gap from ~100 to 300°C in the maximum operating temperatures exists between the $Nd_2Fe_{14}B$- and Sm_2Co_{17}-based permanent magnets. This temperature range covers the exact temperatures that are very critical for many important applications including those in various types of vehicles, magnetic sensors, and transducers and particle-focusing devices.

Since the introduction of sintered Nd-Fe-B magnets in early 1980s [1], extensive studies have been carried out to try to improve the thermal stability of Nd-Fe-B magnets using various approaches, as briefly described below.

(1) Partial substitution of Co for Fe in Nd-Fe-B

Partial substitution of Co for Fe in Nd-Fe-B magnets can effectively increase the Curie temperature of Nd-Fe-B magnets [2, 3]. However, the Co substitution decreases coercivity and significantly increases irreversible loss of magnetic flux.

(2) Partial substitution of Dy and/or Tb for Nd in Nd-Fe-B

Partially substituting Dy and/or Tb for Nd in Nd-Fe-B magnets, on the other hand, effectively increases intrinsic coercivity [2]. However, because both Dy and Tb are heavy rare earths, the coupling in Dy-Fe and Tb-Fe are antiparallel, leading to significantly decreased magnetization. In addition, Dy and Tb are very expensive, resulting in higher magnet cost.

Combining the above two approaches, commercial elevated temperature $(Nd,Dy,Tb)_2(Fe,Co)_{14}B$-based sintered magnets were developed and they demonstrated $(BH)_{max}$ = 28 to 35 MGOe and can be used up to around 150°C. However, this temperature is still lower than what is required in many important applications. In vehicle applications, for example, the under-hood temperature is 180 to 200°C.

(3) Conventional hybrid $Nd_{15}Fe_{79}B_6/Sm_2(Co,Fe,Cu,Zr)_{17}$

Since it is very difficult to increase the operating temperature of a Nd-Fe-B magnet to over 200°C, the third approach is to make a hybrid $Nd_2Fe_{14}B/Sm_2(Co,Fe,Cu,Zr)_{17}$ magnet that may combine the high magnetic performance of $Nd_2Fe_{14}B$ and excellent high temperature stability of $Sm_2(Co,Fe,Cu,Zr)_{17}$. Unfortunately, there are at least two technical difficulties in making this fruitful idea a reality.

(a) Incompatible processes

The process of making sintered Nd-Fe-B magnets is not compatible with that of making sintered $Sm_2(Co,Fe,Cu,Zr)_{17}$ magnets.

- The process of making sintered $Nd_2Fe_{14}B$-based magnets is relatively simple. It includes melting, crushing, milling, powder alignment and compaction, and sintering at around 1080°C for 1 to 2 hours followed by an anneal at around 600°C for 1 hour.
- Sintered $Sm_2(Co,Fe,Cu,Zr)_{17}$ magnets are prepared with a very complex process. After compaction, the green bodies must be sintered at a high temperature of at least 1200°C to reach full density. This sintering temperature is higher than the melting point of $Nd_2Fe_{14}B$. After sintering, a complex and long-term heat treatment procedure must be performed and the entire process lasts for about 3 days.

(b) Interdiffusion between two different types of materials at elevated temperatures

The interdiffusion between $Nd_2Fe_{14}B$ and $Sm_2(Co,Fe,Cu,Zr)_{17}$ will take place during sintering and heat treatments. The possible resulting products from the interdiffusion include $Sm_2Fe_{14}B$, Nd_2Co_{17}, $Nd_2Co_{14}B$, and Sm_2Fe_{17}. Unfortunately, most of these products ($Sm_2Fe_{14}B$, Nd_2Co_{17}, and Sm_2Fe_{17}) have unfavorable easy-basal-plane anisotropy, leading to very low coercivity.

To cope with the difficulties mentioned above, the University of Dayton Magnetics Laboratory proposed to synthesize a new type of hybrid nanocomposite $Pr_2(Fe,Co)_{14}B$/ $Pr(Co,Fe)_5$ permanent magnet. The processes of synthesizing nanocrystalline $Pr_2(Fe,Co)_{14}B$ and $Pr(Co,Fe)_5$ magnet materials are completely compatible. On the other hand, even if there is interdiffusion during the processing, the interdiffusion does not produce any phase that has unfavorable easy basal plane anisotropy.

Prof. Sam Liu of the University of Dayton has proposed an innovative model of coercivity mechanism in magnetic materials with nanograin structure [4]. According to this model, high coercivity can be readily developed in any materials that possess high magnetocrystalline anisotropy, provided these materials are of nanograin structure. Since both $Pr_2Fe_{14}B$ and $PrCo_5$ compounds have high uniaxial magnetocrystalline anisotropy, high coercivity would be readily obtained in $Pr_2Fe_{14}B$ and $PrCo_5$ with nanograin structure. The University of Dayton has also developed the innovative techniques of rapid hot press and hot deformation and has successfully synthesized anisotropic nanocomposite $Nd_2Fe_{14}B/\alpha$-Fe magnets with full density [5, 6]. These techniques were utilized to synthesize anisotropic nanocrystalline $Pr_2(Fe,Co)_{14}B$ and $Pr(Co,Fe)_5$ magnet materials.

2. TECHNICAL APPROACHES

Various technical approaches were used in synthesizing hybrid $Pr_2(Fe, Co)_{14}B/Pr(Co, Fe)_5$ including

- Using rapid hot press and hot deformation to synthesize hybrid nanograin $Pr_2(Fe, Co)_{14}B/Pr(Co, Fe)_5$ magnets
- Using a conventional sintering process to synthesize hybrid micrograin $Pr_2(Fe, Co)_{14}B/Pr(Co, Fe)_5$ magnets
- Using an induction sintering process to synthesize hybrid micrograin $Pr_2(Fe, Co)_{14}B/Pr(Co, Fe)_5$ magnets
- Explore the possibility of synthesizing $Pr_2(Fe,Co)_{14}B/Pr(Co,Fe)_5$ hybrid magnets using a nanoparticle approach.

3. RESULTS AND DISCUSSIONS

3.1 Hybrid Nanograin $Pr_2(Fe,Co)_{14}B/Pr(Co,Fe)_5$ Magnets Synthesized Using Rapid Hot Press and Hot Deformation

3.1.1 Effect of hot deformation temperature on magnetic properties of $PrCo_5$

The techology of synthesing nanograin $Nd_2Fe_{14}B$ magnets using rapid hot press and hot deformation are mature. The same techology can be readily applied to synthesize nanograin $Pr_2Fe_{14}B$. Therefore, the key technical issue is to synthesize nanograin $PrCo_5$ magnets using rapid hot press and hot deformation.

To investigate the effect of hot deformation temperature on grain alignment of $PrCo_5$, a set of mechanically alloyed $PrCo_5$ powder specimens were first hot pressed at 640°C. After hot compaction, these specimens were deformed at 800, 850, 900 and 950°C, respectively. It has been known that good grain alignment can be formed in a broad temperature range of around 800 to 1000°C for $Nd_2Fe_{14}B$. If this is also true for $Pr_2Fe_{14}B$ and if the texture formation in $PrCo_5$ is temperature sensitive, then it would not be too difficult to find a particular temperature that is suitable for both $Pr_2Fe_{14}B$ and $PrCo_5$.

Figures 1 through 4 show demagnetization curves of $PrCo_5$ specimens after hot compaction at 640°C (blue curves) and after hot deformation at 800, 850, 900 and 950°C (red curves), respectively. It can be seen from these figures that all hot compacted specimens have very similar magnetic properties with their $B_r \approx 6.8$ to 6.9 kG, ${}_MH_c \approx 18.1$ to 18.6 kOe, and $(BH)_{max} \approx 10$ to 10.9 MGOe. Specimnes that hot deformed at lower temperature have higher coercivity, but lower energy product. The highest $(BH)_{max}$ of 18.12 MGOe was obtained when hot deformation was performed at 950°C. The $(BH)_{max}$ value of this specimen was increased for 67% after hot deformation, however, its ${}_MH_c$ droped for 62%. Figure 5 summerizes the effect of hot deformation temperature on the magnetic properties of $PrCo_5$ magnets.

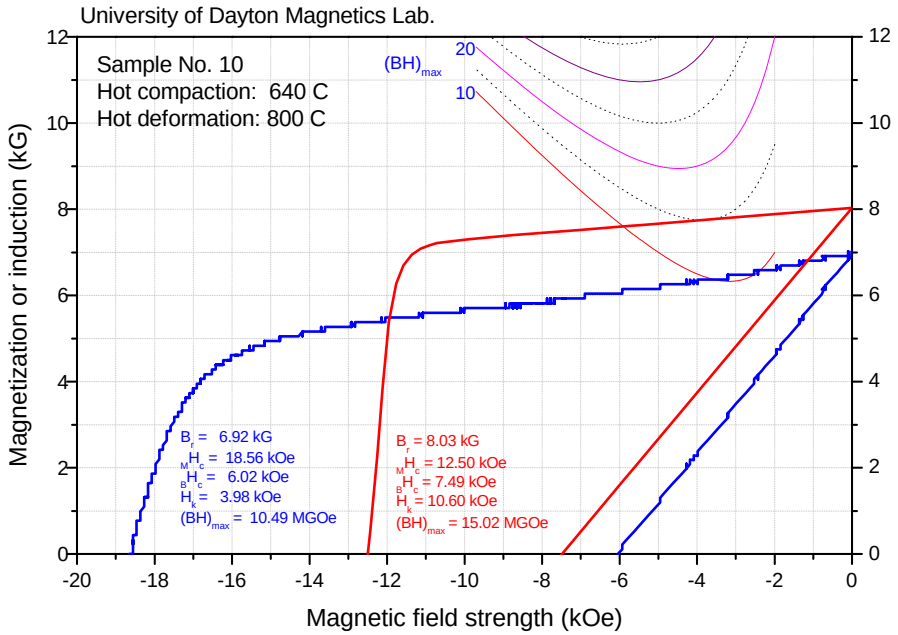

Figure 1. Demagnetization curves of $PrCo_5$ specimen No. 10 after hot compaction at 640°C and hot deformation at 800°C.

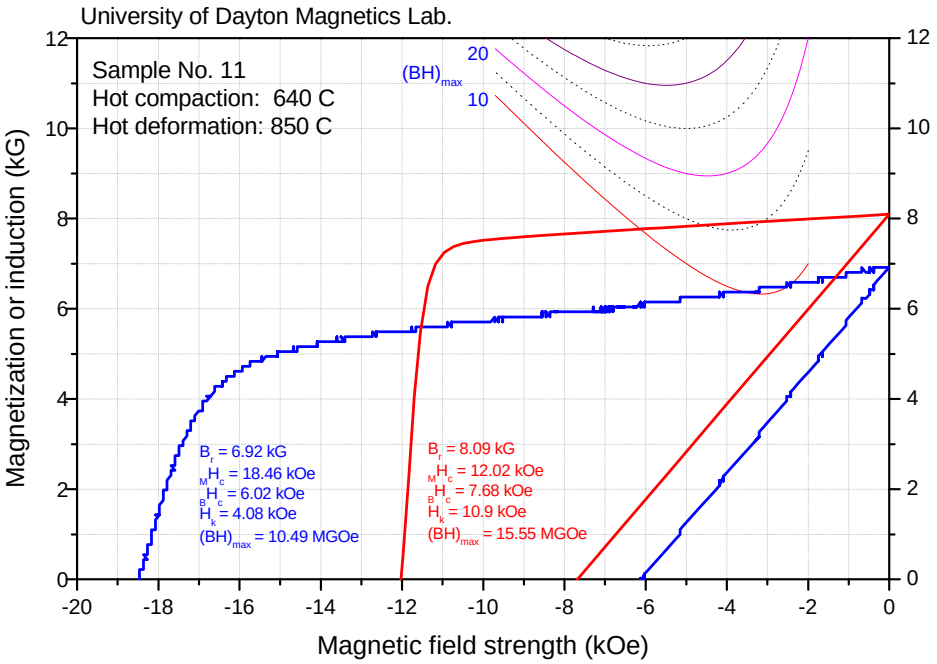

Figure 2. Demagnetization curves of $PrCo_5$ specimen No. 11 after hot compaction at 640°C and hot deformation at 850°C.

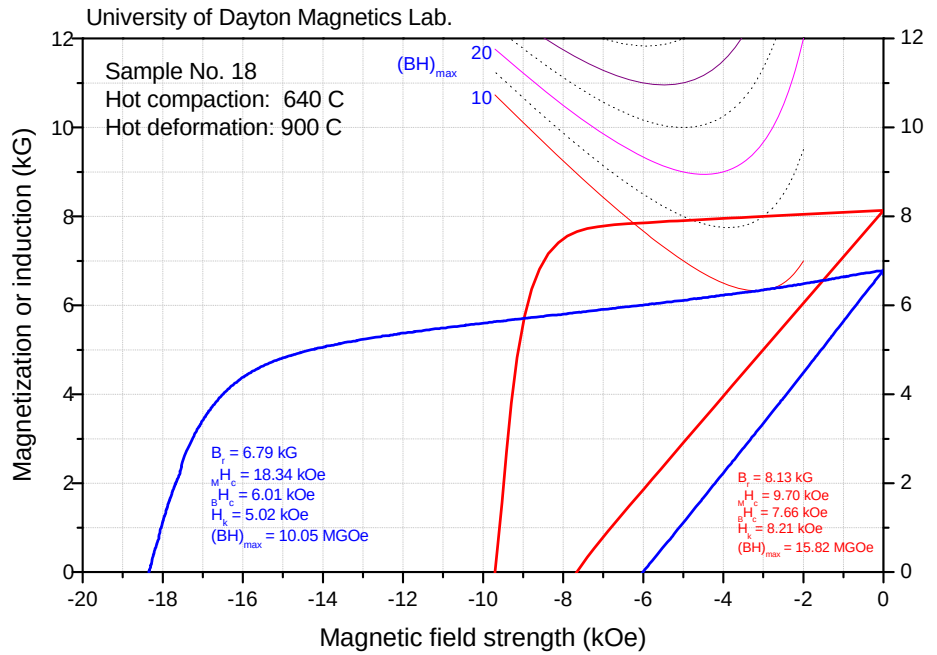

Figure 3. Demagnetization curves of $PrCo_5$ specimen No. 18 after hot compaction at 640°C and hot deformation at 900°C.

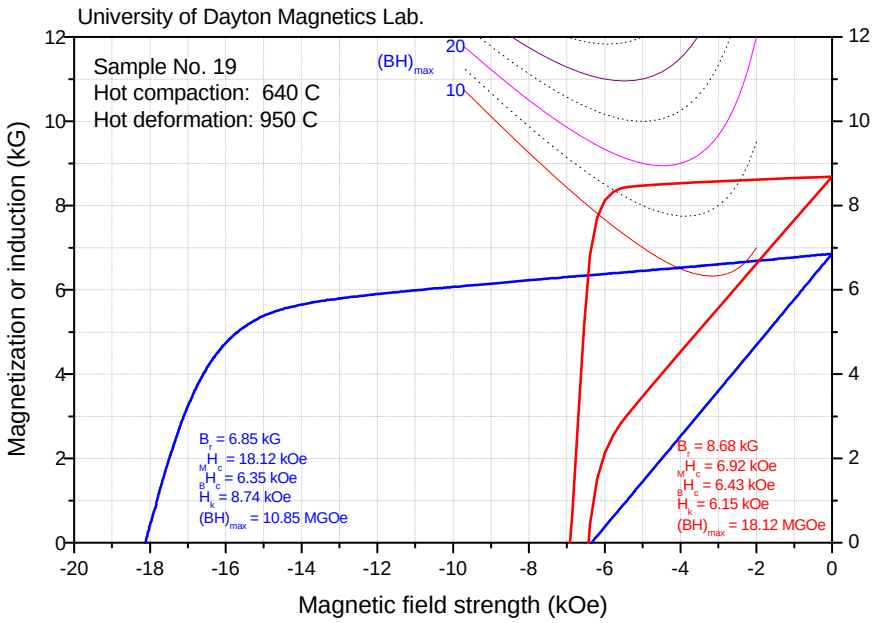

Figure 4. Demagnetization curves of $PrCo_5$ specimen No. 19 after hot compaction at 640°C and hot deformation at 950°C.

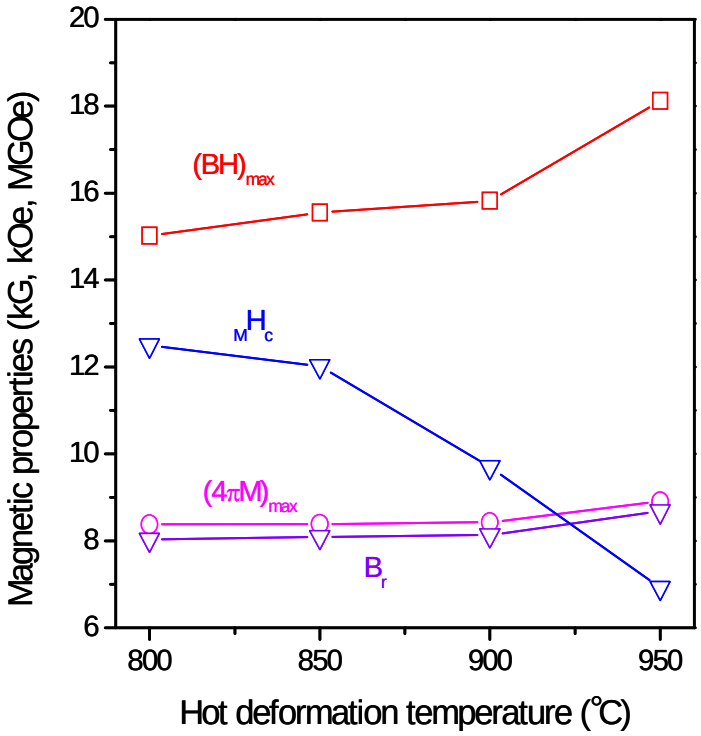

Figure 5. Effect of hot deformation temperature on the magnetic properties of $PrCo_5$ magnets.

3.1.2 Effect of Pr concentration on the magnetic properties of $PrCo_5$

It is well known that the existence of a minor Nd-rich phase is critical for the formation of the desired crystallographic texture in Nd-Fe-B magnets during hot deformation process. Previously, the $PrCo_5$ magnet alloys we studied had a chemical stoichiometric composition without a minor Pr-rich phase. A small amount of Pr-rich phase may help to create the desired grain alignment in $PrCo_5$ during hot deformation, like in the case of Nd-Fe-B.

To verify the effect of a Pr-rich phase, a Pr-rich $PrCo_{4.66}$ magnet alloy powder and a Pr-poor $PrCo_{5.38}$ magnet alloy powder were prepared using mechanical alloying. Then, these powders were hot compacted at 640°C and hot deformed at 950°C. Figures 6 and 7 show demagnetization curves of specimens after hot compaction and hot deformation for the Pr-rich $PrCo_{4.66}$ and Pr-poor $PrCo_{5.38}$ magnets, respectively.

As shown in Figure 6, $PrCo_{4.66}$ has lower B_r and $(BH)_{max}$, but higher ${}_MH_c$ than $PrCo_5$ that hot compacted and hot deformed at the same temperature as shown in Figure 4. Apparently, the minor Pr-rich phase decreases the magnetization and enhances the coercivity. The B_r improvement after hot deformation is 27.8%, similar to the 26.7% for PrCo5 shown in Figure 4. No sign indicates that the grain alignment was improved as a result of the existence of the Pr-rich phase.

It can be seen from Figure 7 that the hot compacted $PrCo_{5.38}$ demonstrates higher B_r and lower ${}_MH_c$ than $PrCo_{4.66}$, while the hot deformed $PrCo_{5.38}$ shows lower B_r and higher ${}_MH_c$ than $PrCo_{4.66}$. The B_r improvement after hot deformation is only 9.92% for $PrCo_{5.38}$.

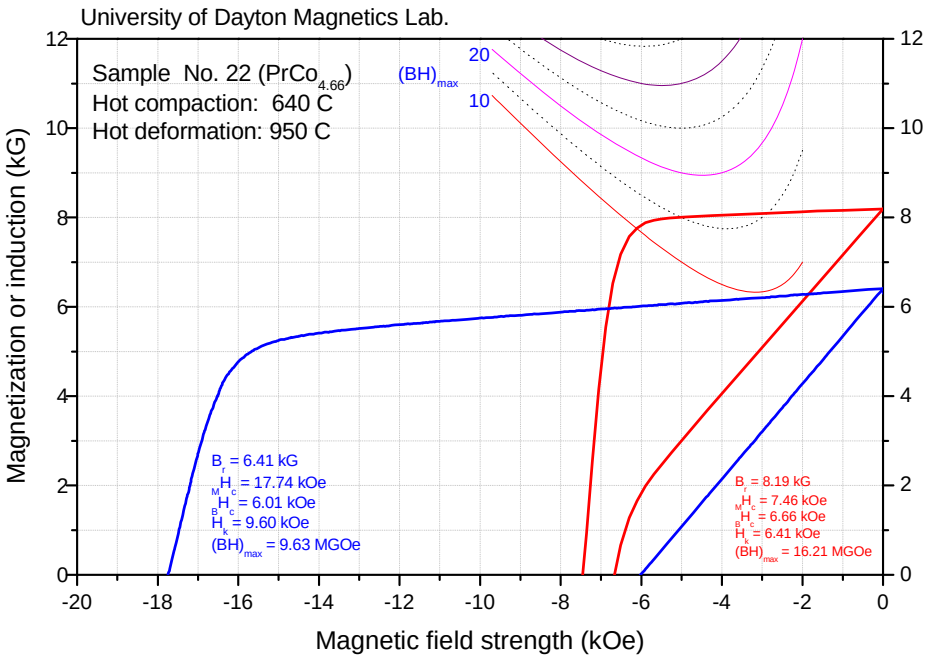

Figure 6. Demagnetization curves of Pr-rich specimen No. 22 ($PrCo_{4.66}$) after hot compaction at 640°C and hot deformation at 950°C.

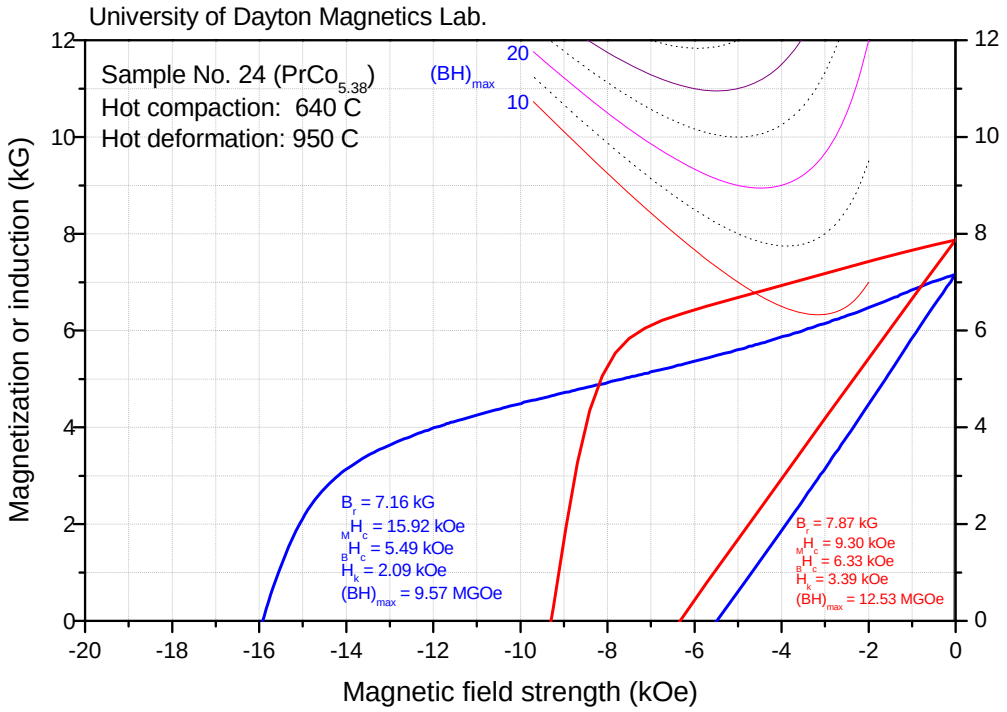

Figure 7. Demagnetization curves of Pr-poor specimen No. 24 ($PrCo_{5.38}$) after hot compaction at 640°C and hot deformation at 950°C.

3.1.3 Effect of hot deformation temperature on the magnetic properties of $Pr_2(Fe,Co)_{14}B$/ $Pr(Co,Fe)_5$ magnets

In order to reveal the effect of hot deformation temperature on the magnetic properties of hybrid $Pr_2(Fe,Co)_{14}B$/ $Pr(Co,Fe)_5$ magnets, $Pr_{14.1}Fe_{73.3}Co_{5.1}Ga_{0.5}B_{7.1}$ and $Pr(Co_{0.8}Fe_{0.2})_5$ alloy powders were prepared by mechanical alloying in Ar for 16 hours. These two powders were then blended at a 80 wt%/20 wt% ratio followed by hot compaction at 580°C. After compaction, the specimens were hot deformed at 760, 830, 890 and 950°C, respectively.

Figures 8 through 11 show demagnetization curves of specimens after hot compaction and hot deformation. As shown in these figures, the highest ${}_MH_c$, B_r, and $(BH)_{max}$ were all obtained when hot deformed at 830°C. Hot deformation at higher temperatures leads to decreased ${}_MH_c$ and $(BH)_{max}$. Figure 12 summarizes the magnetic properties of hybrid $Pr_{14.1}Fe_{73.3}Co_{5.1}Ga_{0.5}B_{7.1}$/ $Pr(Co_{0.8}Fe_{0.2})_5$ (80 wt%/20 wt%) as a function of the hot deformation temperature.

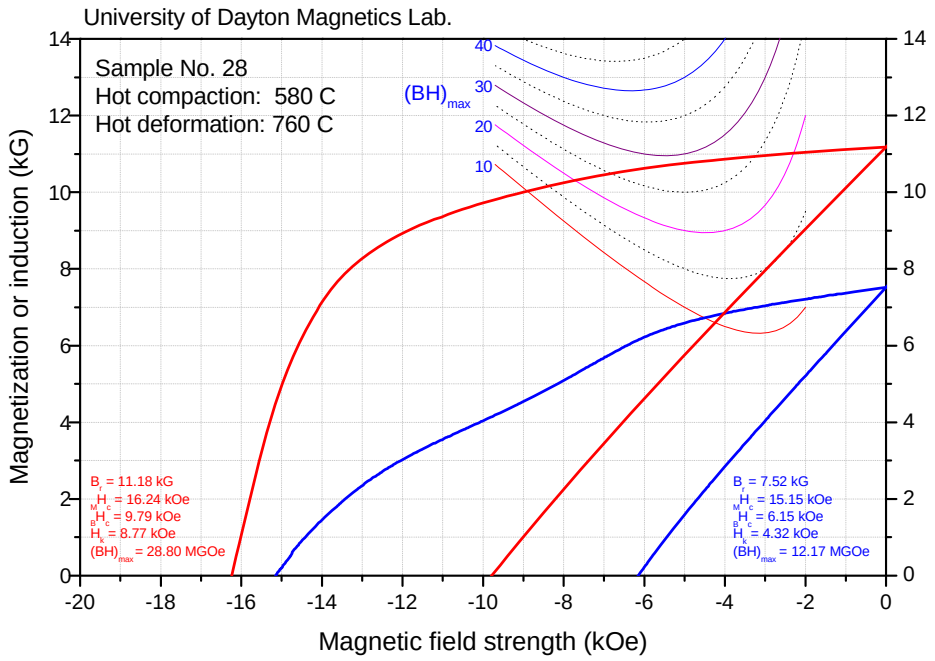

Figure 8. Demagnetization curves of specimen No. 28, $Pr_{14.1}Fe_{73.3}Co_{5.1}Ga_{0.5}B_{7.1}$/ $Pr(Co_{0.8}Fe_{0.2})_5$ (80 wt%/20 wt%), after hot compaction at 580°C and hot deformation at 760°C.

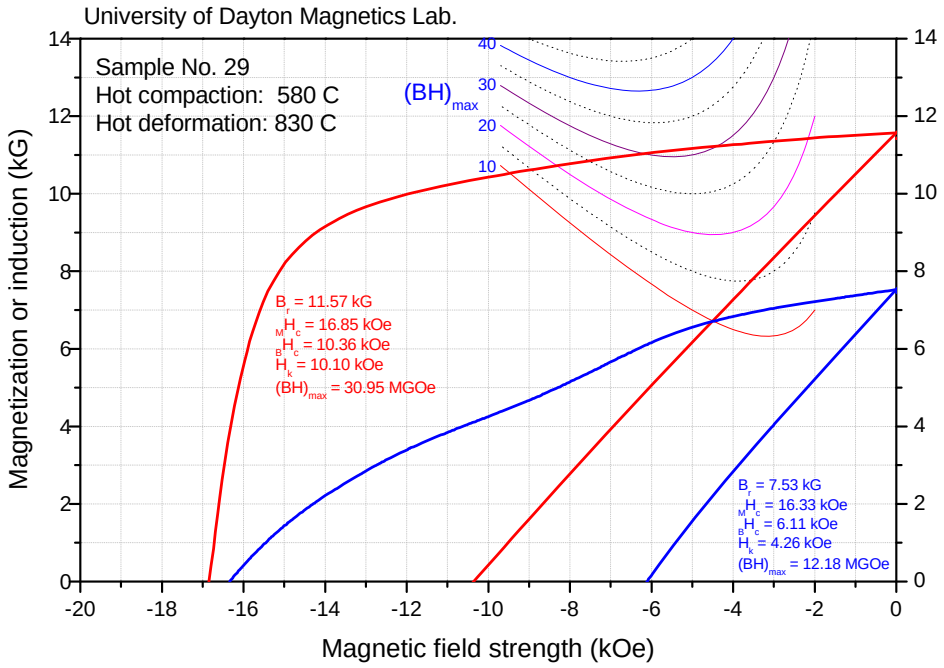

Figure 9. Demagnetization curves of specimen No. 29, $Pr_{14.1}Fe_{73.3}Co_{5.1}Ga_{0.5}B_{7.1}$/ $Pr(Co_{0.8}Fe_{0.2})_5$ (80 wt%/20 wt%), after hot compaction at 580°C and hot deformation at 830°C.

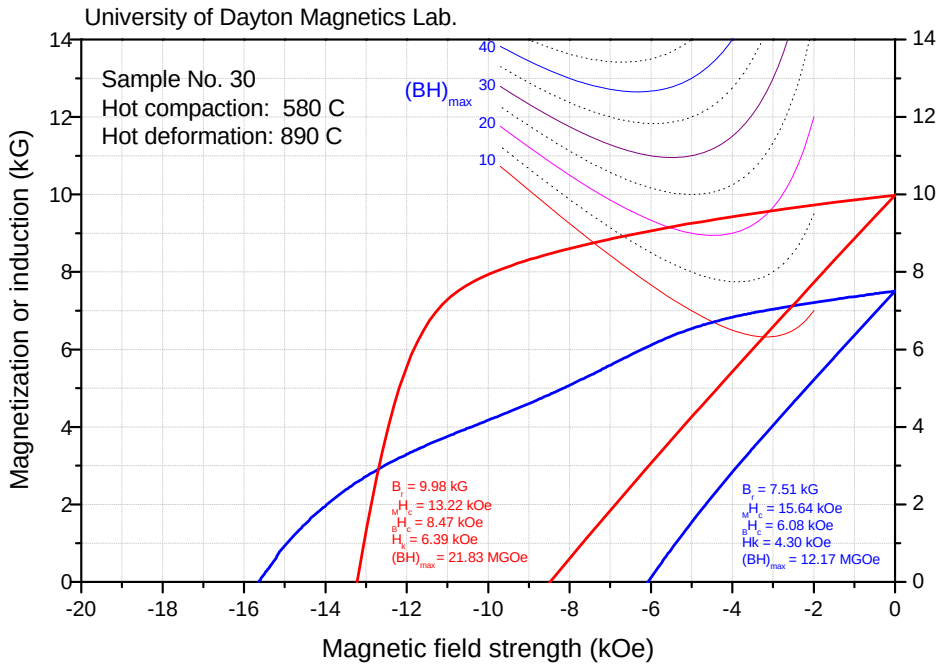

Figure 10. Demagnetization curves of specimen No. 30, $Pr_{14.1}Fe_{73.3}Co_{5.1}Ga_{0.5}B_{7.1}$/ $Pr(Co_{0.8}Fe_{0.2})_5$ (80 wt%/20 wt%), after hot compaction at 580°C and hot deformation at 890°C.

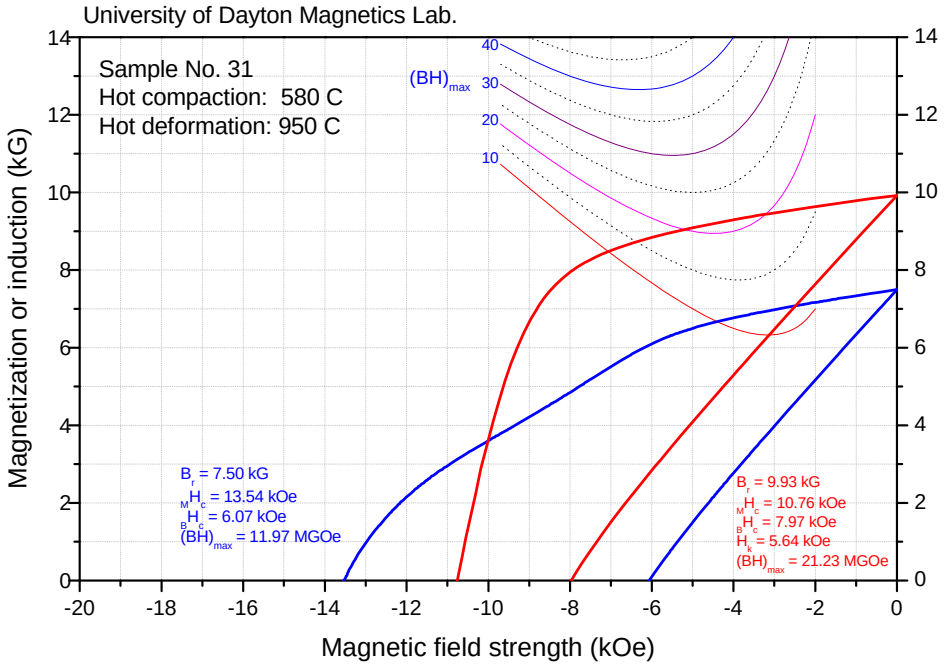

Figure 11. Demagnetization curves of specimen No. 31, $Pr_{14.1}Fe_{73.3}Co_{5.1}Ga_{0.5}B_{7.1}$/ $Pr(Co_{0.8}Fe_{0.2})_5$ (80 wt%/20 wt%), after hot compaction at 580°C and hot deformation at 950°C.

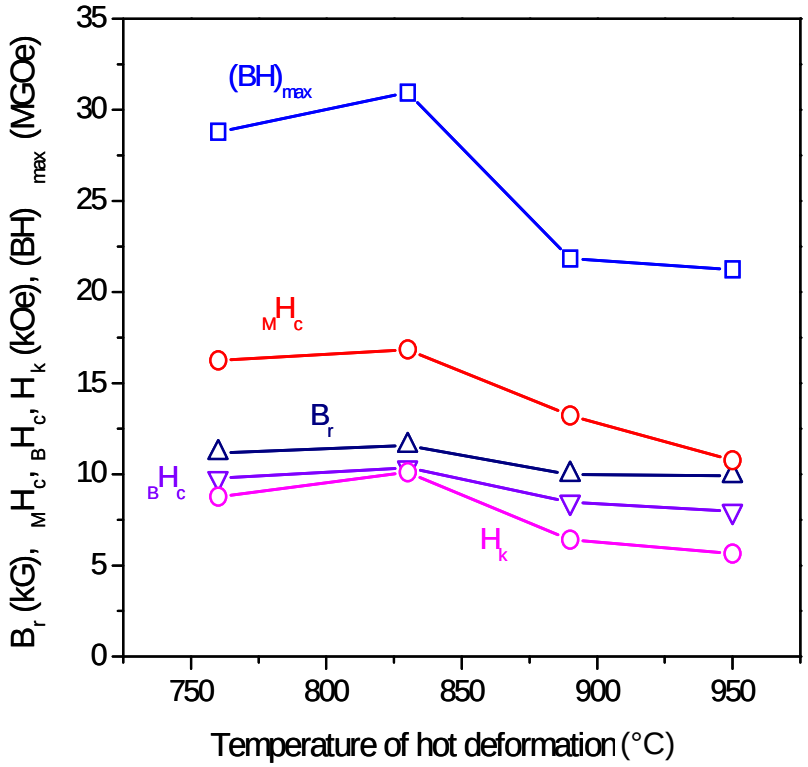

Fig. 12. Magnetic properties vs. hot deformation temperatures for $Pr_{14.1}Fe_{73.3}Co_{5.1}Ga_{0.5}B_{7.1}/Pr(Co_{0.8}Fe_{0.2})_5$ (80 wt%/20 wt%) magnets.

3.1.4 Effect of increasing boron content in the $Pr_2(Fe,Co)_{14}B$ component

In making $Pr_2(Fe,Co)_{14}B/Pr(Co,Fe)_5$ hybrid magnets using sintering process, we observed that increasing the boron content in the $Pr_2(Fe,Co)_{14}B$ component significantly improved the intrinsic coercivity, ${}_MH_c$, knee field, H_k, and, in turn, maximum energy product, $(BH)_{max}$, of hybrid $Pr_2(Fe,Co)_{14}B/Pr(Co,Fe)_5$ magnets. Based on that observation, we increased the boron content in the $Pr_2(Fe,Co)_{14}B$ component when synthesizing hybrid $Pr_2(Fe,Co)_{14}B/ Pr(Co,Fe)_5$ magnets using hot press and hot deformation process.

Table 1 lists magnetic properties of hot pressed and hot deformed hybrid magnets with different boron contents in their $Pr_2(Fe,Co)_{14}B$ components. As shown in Table 1, one magnet contains 7.1 at% boron (#37), while the other one contains 8.1 at% boron (#39). Both magnets were hot pressed at 580°C and hot deformed at 760°C.

It can be seen from Table 1 that two magnets have very similar magnetic properties. The only notable difference is that the magnet that has high boron content demonstrates a higher knee field than its low boron counterpart. It is also worth to mention that the intrinsic coercivity of the hot deformed 39HD is 2 kOe higher than that of the hot pressed 39HP. Demagnetization curves of these two magnets are given in Figure 13.

Table 1. Compositions and Magnetic Properties of Two $Pr_2(Fe,Co)_{14}B/Pr(Co,Fe)_5$ (80wt%/20wt%) Magnets with Different Boron Contents

ID	Composition	B_r (kG)	$_MH_c$ (kOe)	H_k (kOe)	$(BH)_{max}$, (MGOe)
37HP	$Pr_{14.1}Fe_{73.3}Co_{5.1}Ga_{0.5}B_{7.1}/Pr(Co_{0.8}Fe_{0.2})_5$	7.68	>20.86	4.55	12.8
37HD	"	11.63	20.05	10.98	31.88
39HP	$Pr_{14.1}Fe_{72.3}Co_{5.1}Ga_{0.5}B_{8.1}/Pr(Co_{0.8}Fe_{0.2})_5$	7.41	17.23	4.51	11.97
39HD	"	11.5	19.5	12.33	31.38

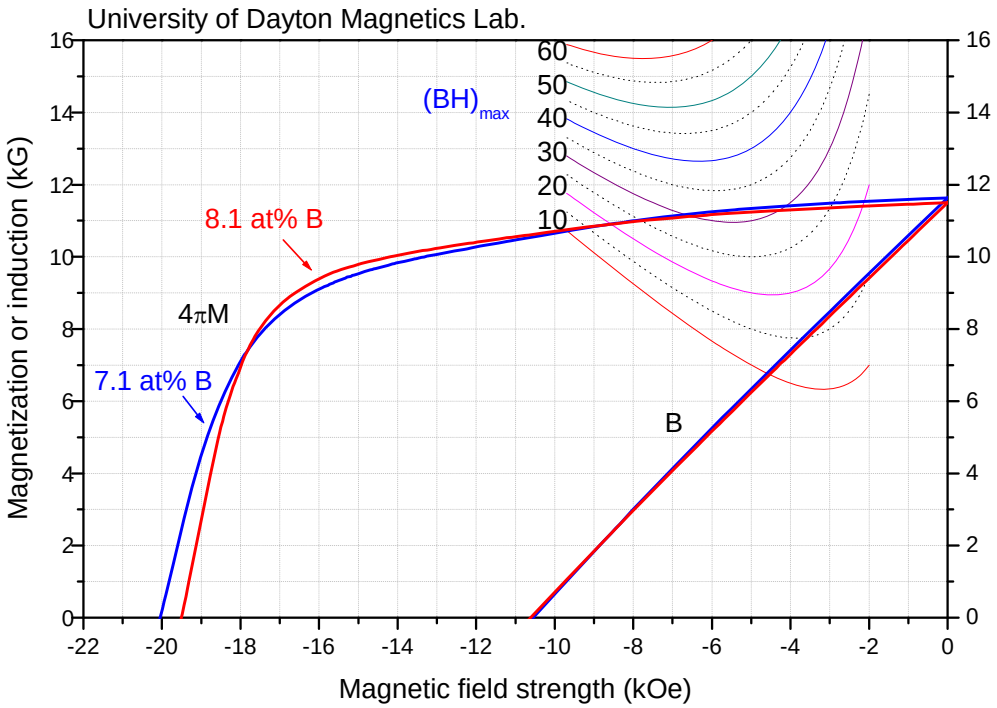

Figure 13. Demagnetization curves of $Pr_{14.1}Fe_{73.3}Co_{5.1}Ga_{0.5}B_{7.1}/Pr(Co_{0.8}Fe_{0.2})_5$ and $Pr_{14.1}Fe_{72.3}Co_{5.1}Ga_{0.5}B_{8.1}/Pr(Co_{0.8}Fe_{0.2})_5$ magnets.

3.1.5 Effect of decreasing Pr content in the $Pr_2(Fe,Co)_{14}B$ component

In an attempt to enhance magnetization of hybrid magnets, we tried to decrease the Pr content in the $Pr_2(Fe,Co)_{14}B$ component from 14.1 at% to 13.6 at%. Figure 14 shows demagnetization curves of $Pr_{14.1}Fe_{72.3}Co_{5.1}Ga_{0.5}B_{8.1}/Pr(Co_{0.8}Fe_{0.2})_5$ (80 wt%/20 wt%) and $Pr_{13.6}Fe_{72.8}Co_{5.1}Ga_{0.5}B_{8.1}/Pr(Co_{0.8}Fe_{0.2})_5$ (80 wt%/20 wt%) magnets, respectively. It is obvious that the magnet with 13.6 at% Pr shows not only much lower $_MH_c$, but also lower B_r and $(BH)_{max}$ than the magnet with 14.1 at% Pr.

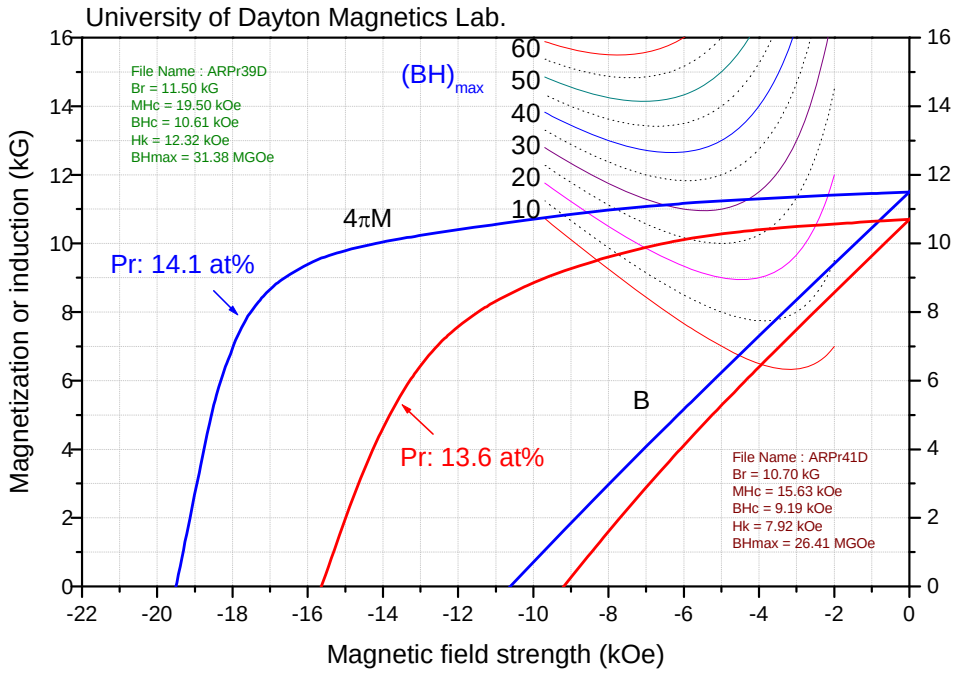

Figure 14. Demagnetization curves of $Pr_{14.1}Fe_{72.3}Co_{5.1}Ga_{0.5}B_{8.1}/Pr(Co_{0.8}Fe_{0.2})_5$ (80 wt%/20 wt%) and $Pr_{13.6}Fe_{72.8}Co_{5.1}Ga_{0.5}B_{8.1}/Pr(Co_{0.8}Fe_{0.2})_5$ (80 wt%/20 wt%) magnets.

The best magnetic property obtained in hybrid nanograin $Pr_2(Fe,Co)_{14}B/Pr(Co,Fe)_5$ (80 wt%/20 wt%) magnets synthesized using hot press and hot deformation was $(BH)_{max}$ = 33.19 MGOe, as shown in Figure 15.

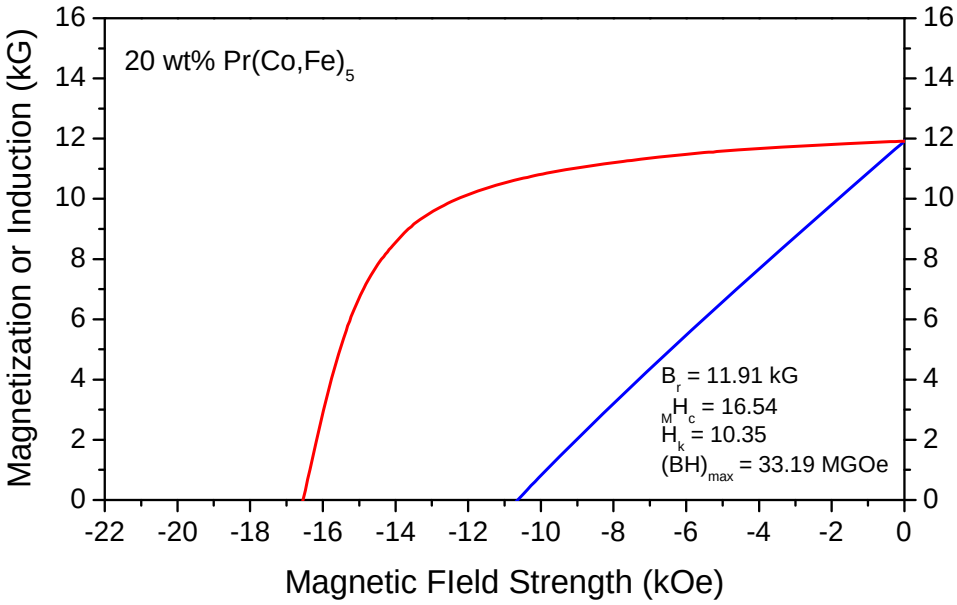

Figure 15. Demagnetization curves of a $Pr_{14.1}Fe_{73.3}Co_{5.1}Ga_{0.5}B_{7.1}/Pr(Co_{0.8}Fe_{0.2})_5$ (80 wt%/20 wt%) magnet with $(BH)_{max}$ = 33.19 MGOe.

3.1.6 Magnetic properties of $Pr_2(Fe,Co)_{14}B/Pr(Co,Fe)_5$ hybrid magnets with 10 wt% of the $Pr(Co,Fe)_5$ component

A hybrid $Pr_{14.1}Fe_{72.3}Co_{5.1}Ga_{0.5}B_{8.1}/Pr(Co_{0.8}Fe_{0.2})_5$ (90 wt%/10 wt%) magnet with 10 wt% 1:5 component was prepared and its magnetic properties was compared with the $Pr_{14.1}Fe_{72.3}Co_{5.1}Ga_{0.5}B_{8.1}/Pr(Co_{0.8}Fe_{0.2})_5$ (80 wt%/20 wt%) magnet with 20 wt% 1:5 component. This comparison is given in Figure 16. As shown in Figure 16, the magnet containing only 10 wt% 1:5 component demonstrates higher B_r, higher $_MH_c$, and higher $(BH)_{max}$ very close to 35 MGOe as compared with the magnet containing 20 wt% 1:5 component.

The best magnetic property obtained in hybrid nanograin $Pr_2(Fe,Co)_{14}B/Pr(Co,Fe)_5$ (90 wt%/10 wt%) magnets synthesized using hot press and hot deformation was $(BH)_{max}$ = 36.85 MGOe, as shown in Figure 17.

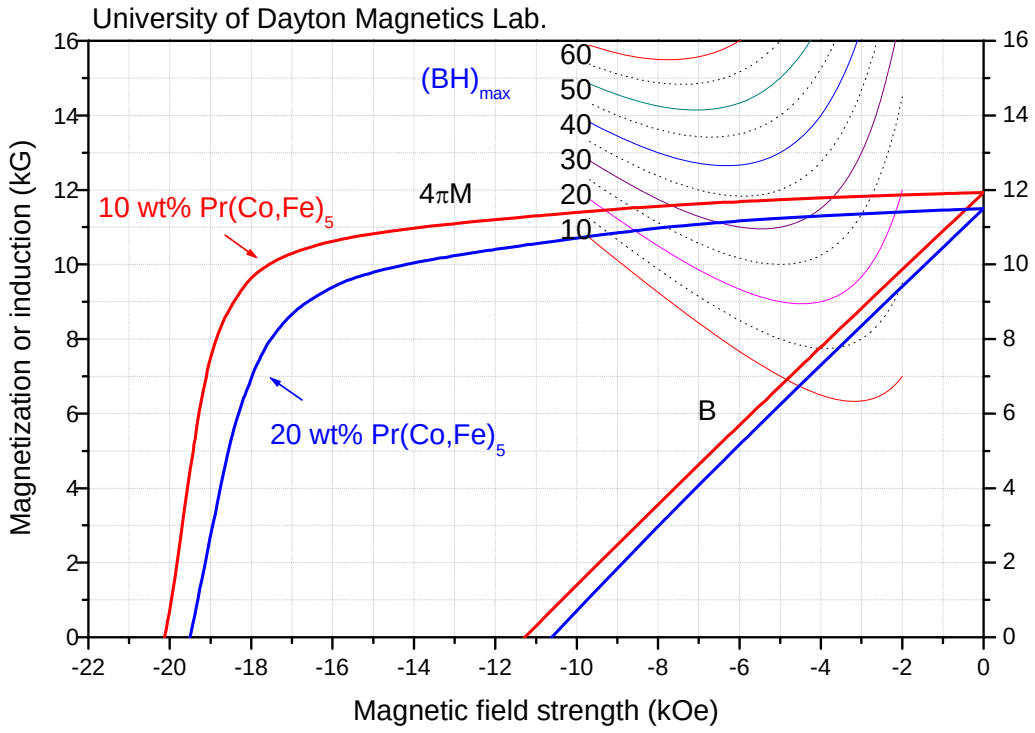

Figure 16. Demagnetization curves of $Pr_{14.1}Fe_{72.3}Co_{5.1}Ga_{0.5}B_{8.1}/Pr(Co_{0.8}Fe_{0.2})_5$ (90 wt%/10 wt%) and of $Pr_{14.1}Fe_{72.3}Co_{5.1}Ga_{0.5}B_{8.1}/Pr(Co_{0.8}Fe_{0.2})_5$ (80 wt%/20 wt%) magnets.

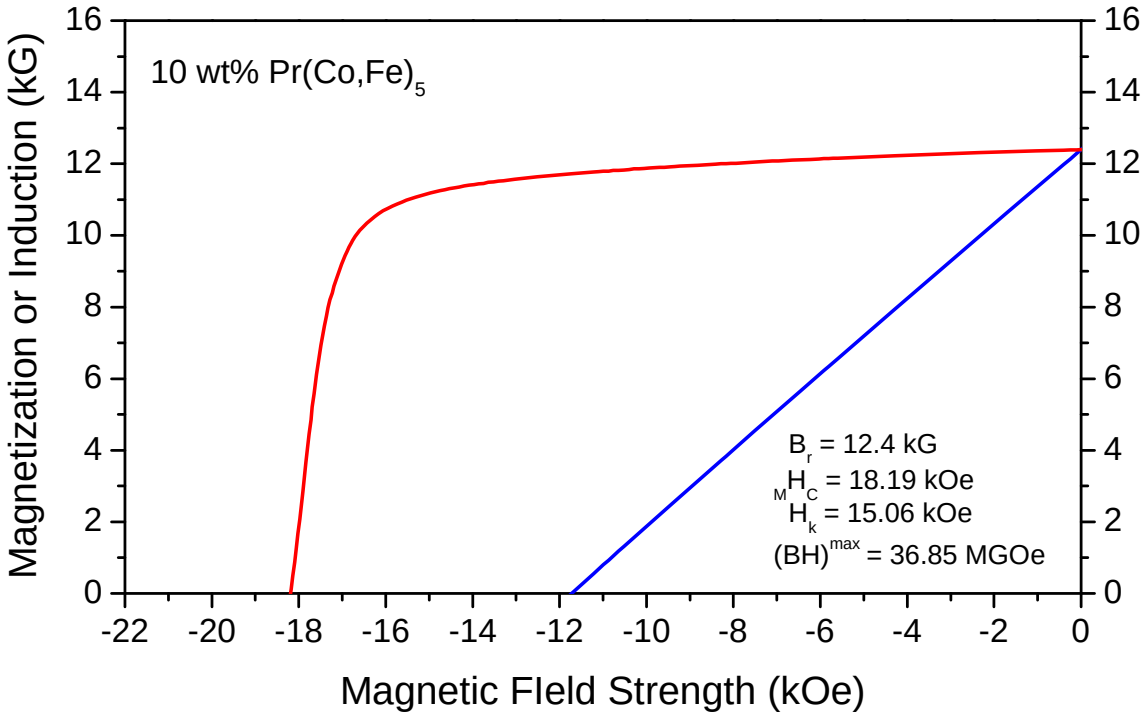

Figure 17. Demagnetization curves of a $Pr_{14.1}Fe_{73.3}Co_{5.1}Ga_{0.5}B_{7.1}/Pr(Co_{0.8}Fe_{0.2})_5$ (90 wt%/10 wt%) magnet with $(BH)_{max}$ = 36.85 MGOe.

3.2 $Pr_2(Fe,Co)_{14}B/Pr(Co,Fe)_5$ Hybrid Magnets Synthesized Using Conventional Sintering Process

3.2.1 Sintered $PrCo_5$ magnets

From Subsection 3.1.1 mentioned above, a preliminary conclusion can be made that by adjusting the hot deformation temperature the grain alignment of a $PrCo_5$ magnet can be partially improved leading to increase B_r and $(BH)_{max}$. For example, after hot deformation at 950°C, the improvements of B_r and $(BH)_{max}$ for a $PrCo_5$ magnet specimen are 26.7% and 67%, respectively, as compared with the hot compacted isotropic magnet specimen. On the other hand, the improvements of B_r and $(BH)_{max}$ for Nd-Fe-B magnets after hot deformation are > 70% and > 200%, respecitively. It would be difficult for a $PrCo_5$ type of magnets to reach that level.

It then becomes necessary to explore the possibility of synthesizing hybrid $Pr_2(Fe,Co)_{14}B/Pr(Co,Fe)_5$ magnets using the conventional powder metallurgy technique. In the conventional powder mettalurgy process, powder magnetic alignment may lead to better grain alignment for the $Pr(Co,Fe)_5$ component than that obtained in the hot deformation process.

Because the $Pr_2(Fe,Co)_{14}B$ component can be readily synthesized using the powder metallurgy technique, the key issue relies on the possibility of producing the $Pr(Co,Fe)_5$ component using the powder metallurgy process.

It is well known that making a sintered $PrCo_5$ magnet is more difficult than making a sintered $SmCo_5$ magnet for at least two reasons. First, the $PrCo_5$ compound is only a line without a homogeneous region in the Pr-Co binary phase diagram, making it very difficult to prepare a single-phased $PrCo_5$ alloy. If the alloy is slightly poor in Pr, then a nonfavorable Pr_2Co_{17} phase will exist leading to low coercivity. On the other hand, if the alloy is silghtly rich in Pr, then a nonfavorable Pr_5Co_{19} or Pr_2Co_7 phase will exist, also leading to low coercivity. Second, $PrCo_5$ is more reactive than $SmCo_5$ and, thus, the oxygen pickup makes the composition control more difficult.

As a first step to exploring the possibility of synthesizing hybrid $Pr_2(Fe,Co)_{14}B$/ $Pr(Co,Fe)_5$ magnets using the powder metallurgy process, sintered $PrCo_5$-type magnet specimens were prepared. Considering the difficulty of composition control and oxygen pick up, a $PrCo_5$ alloy and a $PrCo_{3.5}$ alloy were melted. After crushing, these alloys were ball milled for 5 hours and then blended with the $PrCo_{3.5}$ fraction from 0 up to 100 wt%, followed by powder magnetic alignment and isostatic compaction. The sintering was performed in argon at 1100°C for 1 hour then at 860°C for 40 minutes. In this experiment, three batches of sintered $PrCo_5$ type of magnets with various $PrCo_{3.5}$ fraction were processed and their magnetic properties and density values are listed in Table 2.

It can be seen from Table 2 that these magnet samples have very low intrinsic coercivity. The highest ${}_MH_c$ is only 1.08 kOe (specimen 25); however, their B_r is quite high. A lot of specimens have B_r greater than 10 kG and the highest B_r is 11.02 kG, much higher than the highest B_r value of 8.68 kG obtained using hot deformation. This result clearly indicates that significant improvement of grain alignment can be obtained by using powder magnetic alignment in a powder metallurgy process. Actually, as shown in Table 2, a lot of specimens demonstrate a high degree of grain alignment greater than 90%. The highest degree of grain alignment obtained in this experiment is 94.7% (specimen 17), which is at the same level of the best sintered Nd-Fe-B magnets and better than the best hot deformed Nd-Fe-B magnets.

SEM was used to observe the microstructure of one of the sintered $PrCo_5$ magnet specimen (No. 19) and Figure 18 (a, b) demonstrates the second electron image and the back scattered electron image, respectively, showing at least two phases in the magnet. The SEM/EDS analysis was performed and its result was given in Figure 19 and Table 3, which revealed that the matrix phase is a $PrCo_5$ phase, while the white spots shown in Figure 18 are rich in Pr and poor in Co.

Table 2. Magnetic Properties of Sintered $PrCo_5$ Magnets

No.	wt% of $PrCo_{3.5}$	B_r (kG)	$_MH_c$ (kOe)	$_BH_c$ (kOe)	H_k (kOe)	$(BH)_{max}$ (MGOe)	Alignment (%)	Density (g/cm^3)
6	0	9.59	0.68	0.67	0.47	4.07	87.59	8.05
7	3	9.72	0.67	0.66	0.51	4.28	88.07	8.05
8	6	9.73	0.73	0.72	0.55	4.61	87.98	8.02
9	9	9.75	0.77	0.77	0.58	4.98	87.79	8.00
10	12	10.07	0.81	0.81	0.64	5.44	88.78	8.06
11	15	10.20	0.82	0.81	0.64	5.55	89.80	8.06
12	18	10.12	0.71	0.70	0.49	4.20	91.40	7.98
13	0	9.25	0.94	0.92	0.62	5.01	87.46	7.48
14	6	9.76	0.83	0.82	0.63	5.29	89.55	7.61
15	12	9.93	0.61	0.60	0.46	3.97	90.03	7.75
16	18	10.31	0.40	0.40	0.23	2.25	91.76	7.93
17	24	10.82	0.24	0.24	0.11	1.29	94.73	7.97
18	30	10.83	0.57	0.56	0.32	3.14	92.80	7.92
19	36	11.02	0.85	0.83	0.59	5.58	92.29	8.05
20	50	10.71	0.81	0.80	0.70	6.37	93.46	8.19
21	60	10.27	0.72	0.71	0.55	4.83	94.06	8.18
22	70	9.75	0.72	0.71	0.65	5.27	92.51	8.19
23	80	9.38	0.75	0.74	0.68	5.31	91.15	8.19
24	90	8.81	0.87	0.86	0.73	5.27	89.22	8.22
25	100	8.07	1.08	1.00	0.63	4.23	85.13	8.16

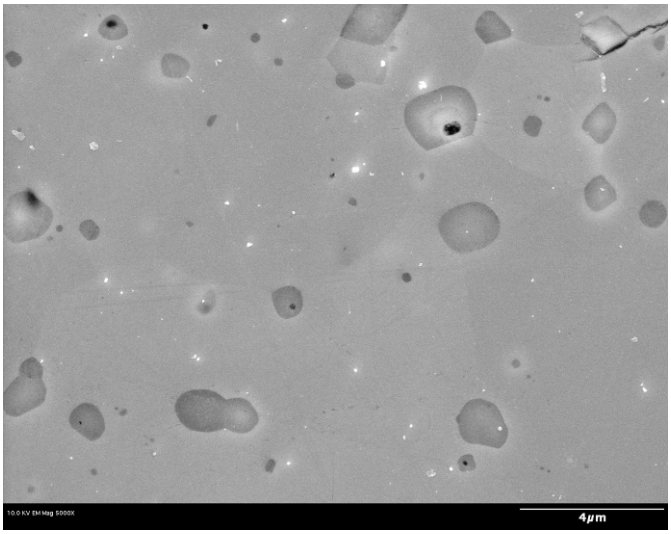

(a)

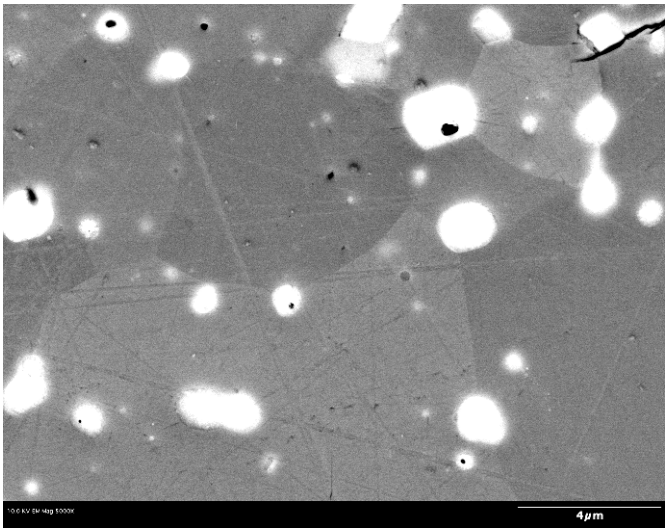

(b)

Figure 18. SEM micrographs of a $PrCo_5$ type of magnet sample (No.19).
(a) Second electron image; (b) back scattered electron image.

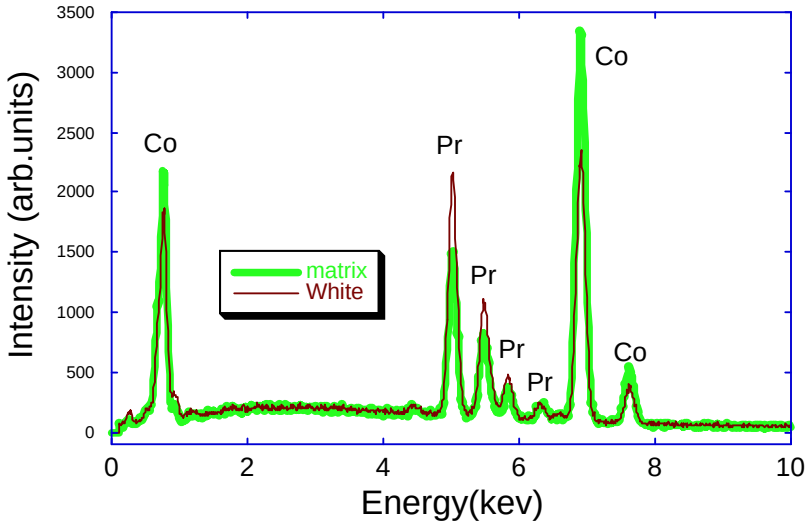

Figure 19. Result of SEM/EDS analysis for specimen No. 19.

Table 3. Compositions of Each Phase Obtained from SEM/EDS Analysis for Specimen No. 19

	Co (at%)	Pr (at%)	3d/R Ratio
White spot in Figure 18	71.9	28.0	~2.6
Matrix	83.9	16.1	~5.2

Thermogravimetry analysis (TGA) was performed on Specimen No. 22, which reveals a few events at 407, 551, 599 and 912°C, respectively, as shown in Figure 20. The major event at 599°C corresponds to the Curie temperature of the main $PrCo_5$ phase, while minor events at 407 and 912°C probably correspond to Curie temperatures of minor Pr_5Co_{19} and Pr_2Co_{17} phases. Apparently, efforts need to be made to adjust the alloy composition to eliminate all minor phases existing currently in $PrCo_5$ type magnet specimens.

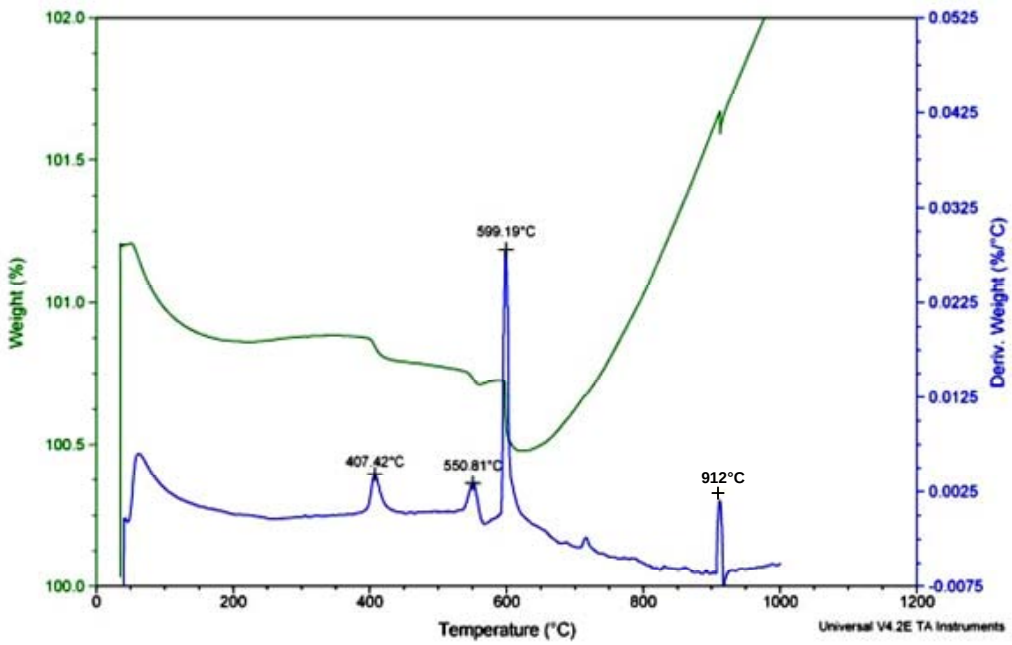

Figure 20. TGA result of specimen No. 22.

3.2.2 Magnetic properties of sintered $Pr_2(Fe,Co)_{14}B$, $PrCo_5$, and $Pr(Co,Fe)_5$ magnets

Sintered $Pr_2(Fe,Co)_{14}B$, $PrCo_5$, and $Pr(Co,Fe)_5$ magnets were made using a powder metallurgy process. The alloys were first prepared by arc melting under argon. After crushing, fine powders with particles size of approximately 3 to 5 micometers were prepared by ball milling for 3 hours. Then, the powders were first loaded into rubber molds followed by magnetic alignment and isostatic pressing at 3 tons/cm^2. Finally, the green bodies were sintered at 1030°C for 1 hour and annealed at 580°C for 20 minutes, as a post-sintering heat treatment.

Figure 21 shows demagnetization curves of a sintered $Pr_{17}Fe_{64.75}Co_{10}Al_{0.25}B_8$ magnet with good magnetic properties of $(BH)_{max} \approx 30$ MGOe, which is not too far from nanograin Pr-Fe-B magnets prepared by hot compaction and hot deformation. Figure 22 shows demagnetization curves of sintered $PrCo_5$ and $Pr(Co_{0.8}Fe_{0.2})_5$ magnets. Different from the case in Pr-Fe-B, the sintered PCo_5 demonstrates poor magnetic performance (especially low coercivity) as compared with that prepared by hot compaction and hot deformation – shown in Figure 23. Fe substituted $Pr(Co_{0.8}Fe_{0.2})_5$ shows even worse properties with ${}_MH_c = 0.19$ kOe and $(BH)_{max} = 0.21$ MGOe!

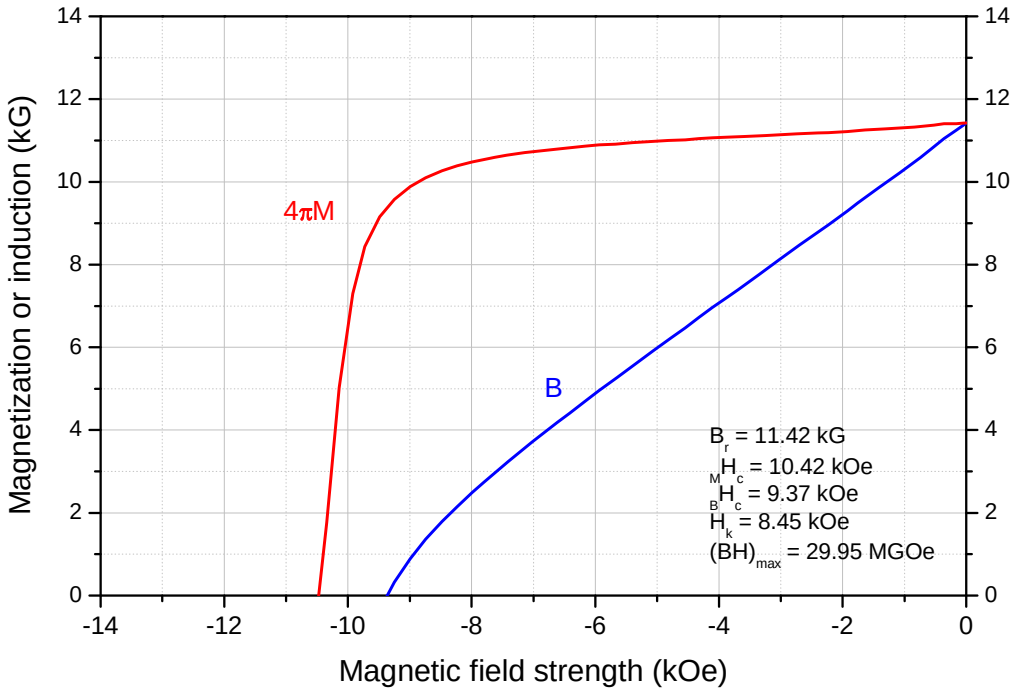

Figure 21. Demagnetization curves of a sintered $Pr_{17}Fe_{64.75}Co_{10}Al_{0.25}B_8$ magnet.

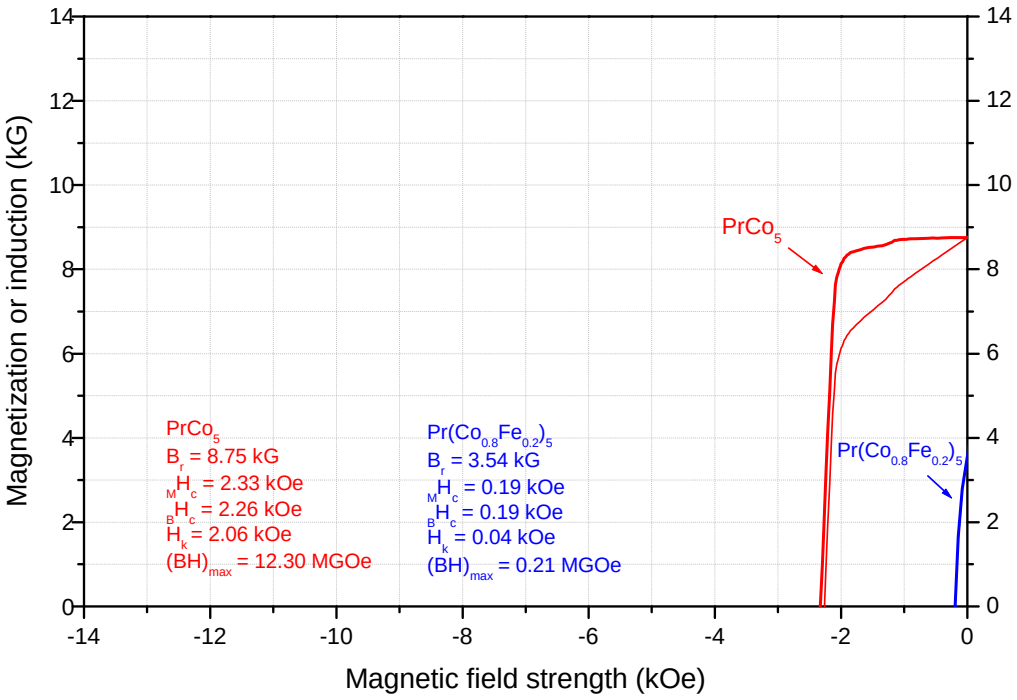

Figure 22. Demagnetization curves of sintered $PrCo_5$ and $Pr(Co_{0.8}Fe_{0.2})_5$ magnets.

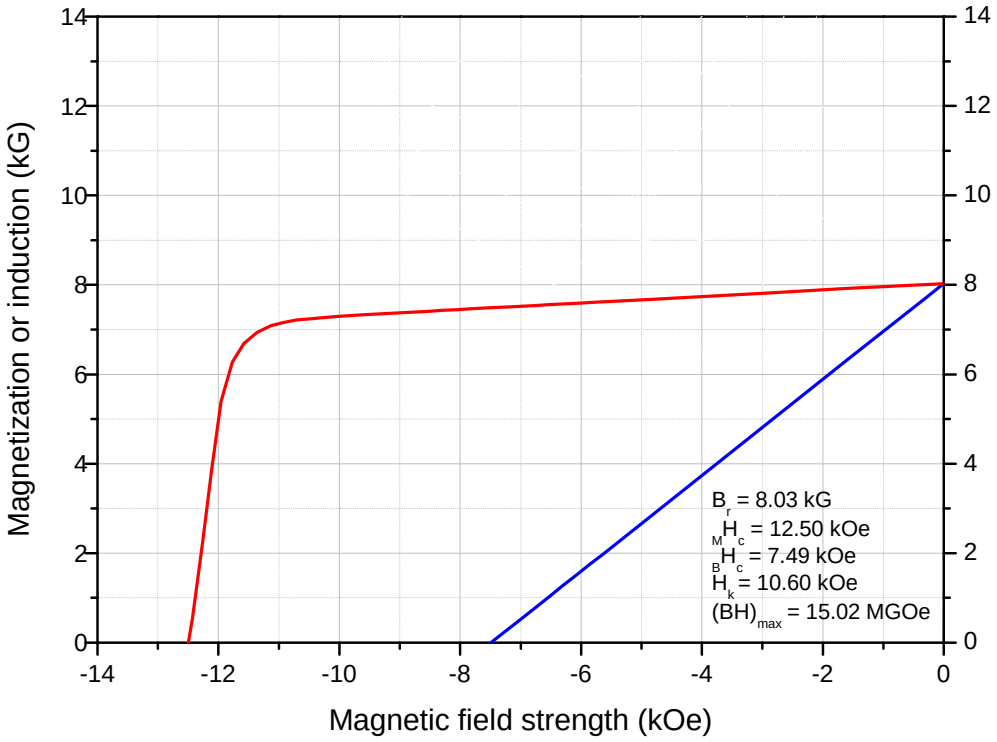

Figure 23. Demagnetization of a nanograin $PrCo_5$ magnet hot compacted at 640°C and hot deformed at 800°C.

3.2.3 Sintered hybrid $Pr_2(Fe,Co)_{14}B/PrCo_5$ and $Pr_2(Fe,Co)_{14}B/Pr(Co,Fe)_5$ magnets

For making hybrid $Pr_2(Fe,Co)_{14}B/PrCo_5$ and $Pr_2(Fe,Co)_{14}B/Pr(Co,Fe)_5$ magnets**,** 80 wt% of $Pr_2(Fe,Co)_{14}B$ fine powder was blended with 20 wt% $PrCo_5$ or $Pr(Co,Fe)_5$ fine powder followed by magnetic alignment, isostatic compaction, sintering, and post-sintering heat treatment.

Figure 24 shows demagentization curves of $Pr_{17}Fe_{68.21}Co_{8.5}Al_{0.19}B_{6.1}/PrCo_5$ and $Pr_{17}Fe_{68.21}Co_{8.5}Al_{0.19}B_{6.1}/Pr(Co_{0.8}Fe_{0.2})_5$ magnets. The fractions of the $PrCo_5$ or $Pr(Co_{0.8}Fe_{0.2})_5$ component for both magnets are 20 wt%. Though a single $Pr(Co_{0.8}Fe_{0.2})_5$ has much worse performance then $PrCo_5$, both hybrid magnets demonstrate very similar magnetic properties. Actually, $Pr_{17}Fe_{68.21}Co_{8.5}Al_{0.19}B_{6.1}/Pr(Co_{0.8}Fe_{0.2})_5$ has slightly better performance than $Pr_{17}Fe_{68.21}Co_{8.5}Al_{0.19}B_{6.1}/PrCo_5$, as shown in Figure 24. This interesting phenomenon is believed to be related to the interdiffusion during the high-temperature sintering process.

The Pr-Fe-B component of both magnets has a low boron content of 6.1 at%, which leads to poor squareness of the demagnetization curve. This can be explained by the formation of an unfavorable Pr_2Fe_{17} phase under a boron depleted environment.

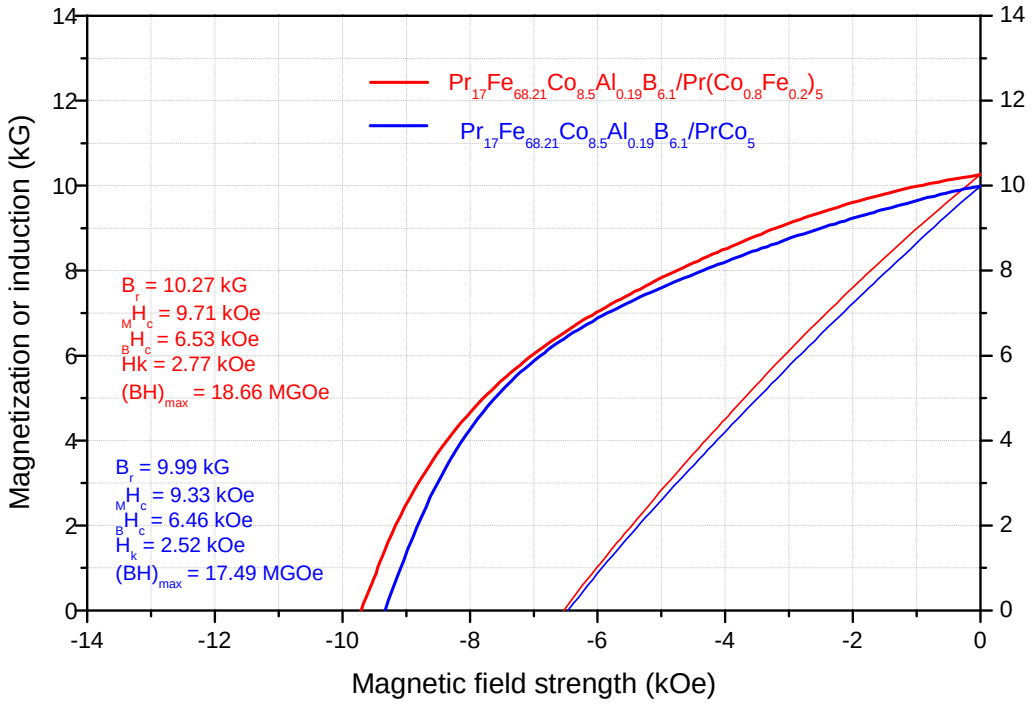

Figure 24. Demagnetization curves of $Pr_{17}Fe_{68.21}Co_{8.5}Al_{0.19}B_{6.1}/PrCo_5$ and $Pr_{17}Fe_{68.21}Co_{8.5}Al_{0.19}B_{6.1}/Pr(Co_{0.8}Fe_{0.2})_5$ magnets.

3.2.4 Effect of sintering time at 1030°C on the magnetic properties of sintered $Pr_{17}Fe_{68.21}Co_{8.5}Al_{0.19}B_{6.1}$ magnets

In these experiments, all sintering was performed at a relatively low temperature of 1030°C to avoid significant interdiffusion. Figure 25 shows the sintering time on the magnetic properties of sintered $Pr_{17}Fe_{68.21}Co_{8.5}Al_{0.19}B_{6.1}$ magnets. When the sintering time is increased from 1 to 2 hours, both intrinsic coercivity and remanence were slightly enhanced, while the maximum energy product was increased for 19%. Further, magnetic performance basically remains the same when the sintering time is extended to 3 hours. These experimental results indicate that a higher sintering temperature can be used in the future, which will further increase the specimen density and, in turn, the magnetic properties.

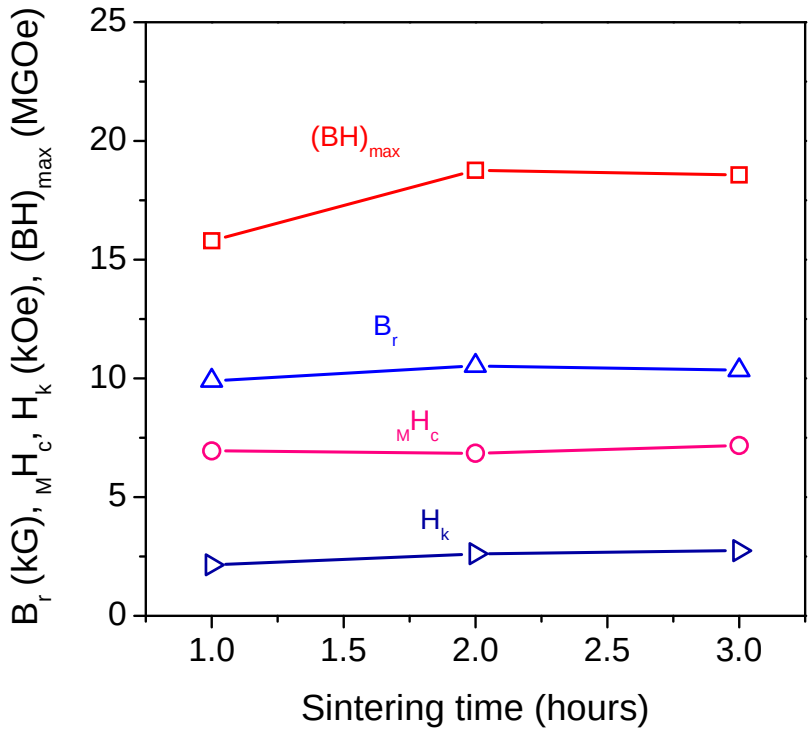

Figure 25. Effect of sintering time on the magnetic properties of sintered $Pr_{17}Fe_{68.21}Co_{8.5}Al_{0.19}B_{6.1}$ magnets.

3.2.5 Effect of post-sintering heat treatment at 580°C on the magnetic properties of sintered $Pr_{17}Fe_{68.21}Co_{8.5}Al_{0.19}$ $B_{6.1}$ magnets

Figure 26 shows demagnetization curves of a sintered $Pr_{17}Fe_{68.21}Co_{8.5}Al_{0.19}$ $B_{6.1}$ magnet in the as-sintered condition and after heat-treating at 580°C for 20 minutes, 1 hour and 20 minutes, and 2 hours and 20 minutes. After heat treating for 1 hour 20 minutes, the intrinsic coercivity value increases by a sizeable 36.2%. No improvement was observed after further increasing the time to 2 hours and 20 minutes.

Variations of the magnetic properties as a function of the post-sintering heat treatment time are summarized in Figure 27. It can be seen from Figure 27 that magnetic properties of sintered $Pr_{17}Fe_{68.21}Co_{8.5}Al_{0.19}$ $B_{6.1}$ magnets are not very sensitive to the time of the post-sintering heat treatment and it seems that when the heat treatment was performed for 80 minutes the magnets demonstrate the best magnetic properties.

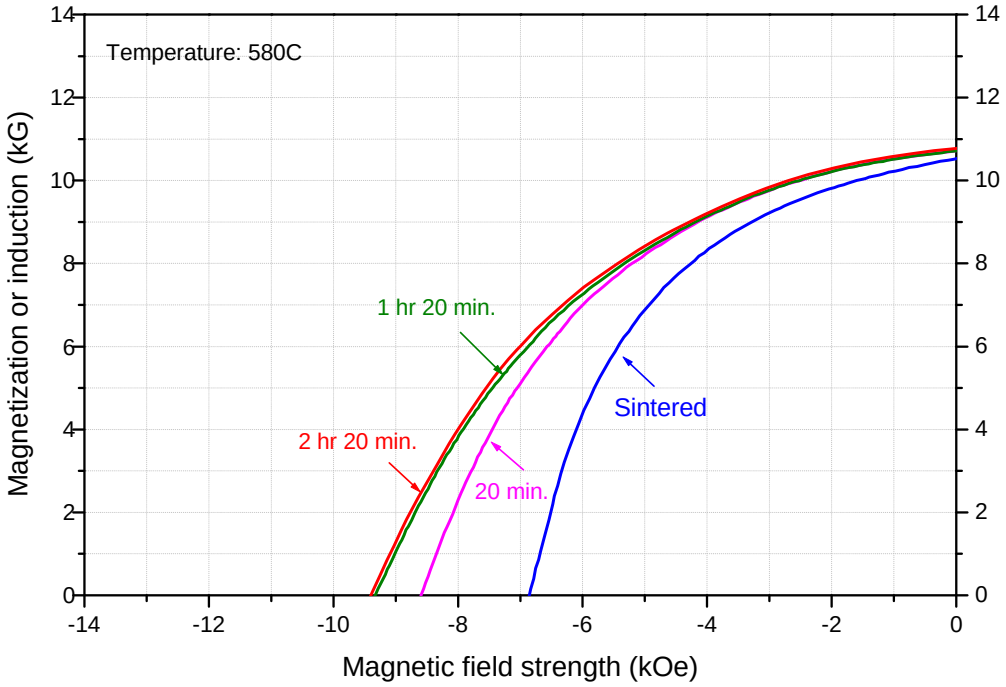

Figure. 26. Demagnetization curves of sintered $Pr_{17}Fe_{68.21}Co_{8.5}Al_{0.19}$ $B_{6.1}$ magnets heat treated for different times.

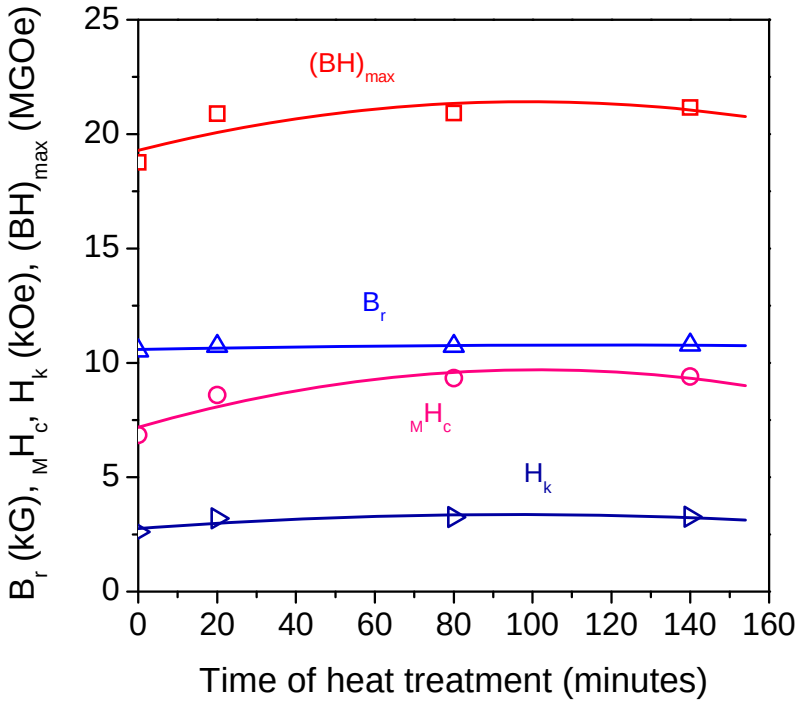

Figure 27. Effect of time for post-sintering heat treatment at 580°C on the magnetic properties of sintered $Pr_{17}Fe_{68.21}Co_{8.5}Al_{0.19}B_{6.1}$ magnets.

3.2.6 Effect of boron content on magnetic properties of sintered $Pr_2Fe_{14}B$ and $Pr_2Fe_{14}B$/ $Pr(Co,Fe)_5$ based magnets

Figure 28 shows demagnetization curves of a sintered $Pr_{17}Fe_{68.21}Co_{8.5}Al_{0.19}B_{6.1}$ magnet and a sintered $Pr_{17}Fe_{66.31}Co_{8.5}Al_{0.19}B_8$ magnet. The only difference between these two magnets is that the second magnet comprises a higher boron content. Increasing the boron content significantly improves magnetic properties of the hybrid magnet. Compared to the magnet specimen containing 6.1 at% of B, the increase of ${}_MH_c$, H_k, and $(BH)_{max}$ for the magnet specimen with 8 at% are 32.5%, 126.5%, and 21.7%, respectively.

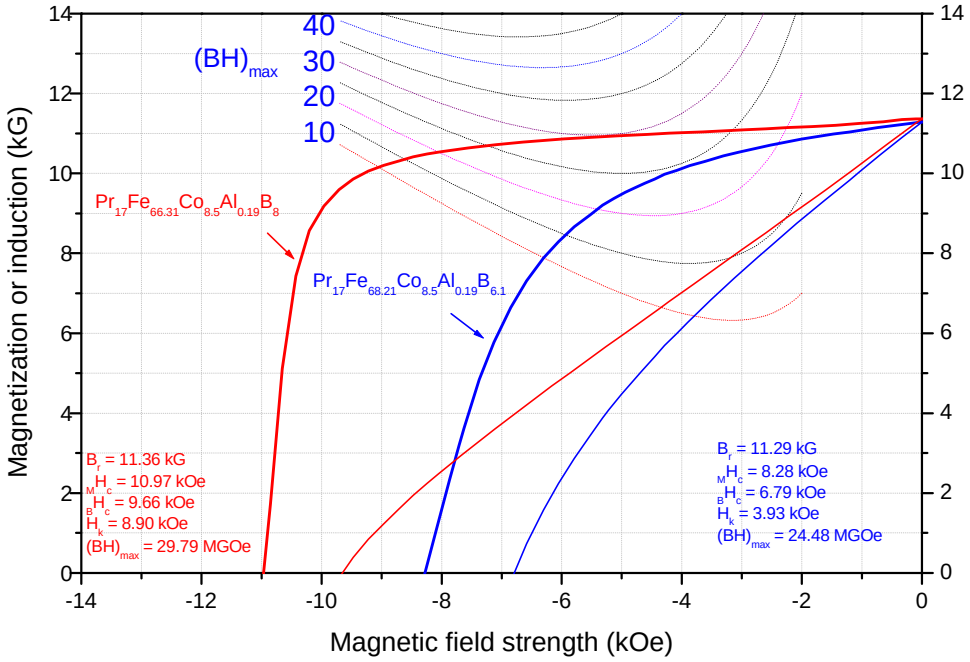

Figure 28. Comparison of demagnetization curves of sintered $Pr_{17}Fe_{68.21}Co_{8.5}Al_{0.19}B_{6.1}$ (blue curves) and $Pr_{17}Fe_{64.75}Co_{10}Al_{0.25}B_8$ (red curves) magnets.

Figure 29 summarizes the effects of boron content, x, on the magnetic properties of hybrid $Pr_{17}Fe_{74.31-x}Co_{8.5}Al_{0.19}B_x/Pr(Co_{0.8}Fe_{0.2})_5$ magnets containing 20 wt% of the $Pr(Co_{0.8}Fe_{0.2})_5$ phase. The peak $(BH)_{max}$ value is observed when the boron content in the Pr-Fe-B component is 8 at%. When the boron content is increased from 6.1 at% to 8 at%, increases of ${}_MH_c$, H_k, and $(BH)_{max}$ are 12.2, 193.4 and 56.4%, respectively. These significant improvements can be explained by the fact that sufficiently high boron content prevents the formation of an unfavorable Pr_2Fe_{17} and/or Pr_2Co_{17} phase. This assumption is yet to be confirmed in future research using x-ray diffraction (XRD) coupled by SEM-EDS analyses.

Demagnetization curves of the best sintered hybrid $Pr_2(Fe,Co)_{14}B/Pr(Co,Fe)_5$ (80 wt%/20 wt%) magnet obtained are given in Figure 30. Its maximum energy product reaches 30 MGOe, the same level as nanograin hybrid magnets, while the squareness of the demagnetization curve is much better than the nanograin hybrid magnet with the same composition. However, the intrinsic coercivity of sintered hybrid magnets needs to be further enhanced so that the induction demagnetization curve (B curve) can be linear without a knee, which is critical for all dynamic applications.

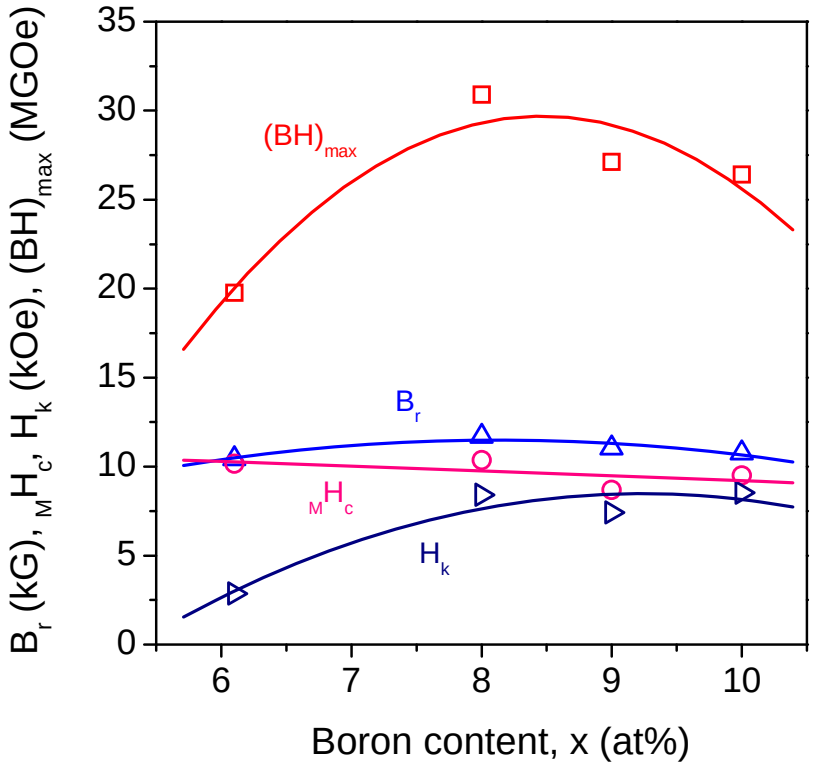

Figure 29. Magnetic properties as a function of boron content for sintered hybrid $Pr_{17}Fe_{74.31-x}Co_{8.5}Al_{0.19}B_x/Pr(Co_{0.8}Fe_{0.2})_5$ magnets (80 wt%/20 wt%).

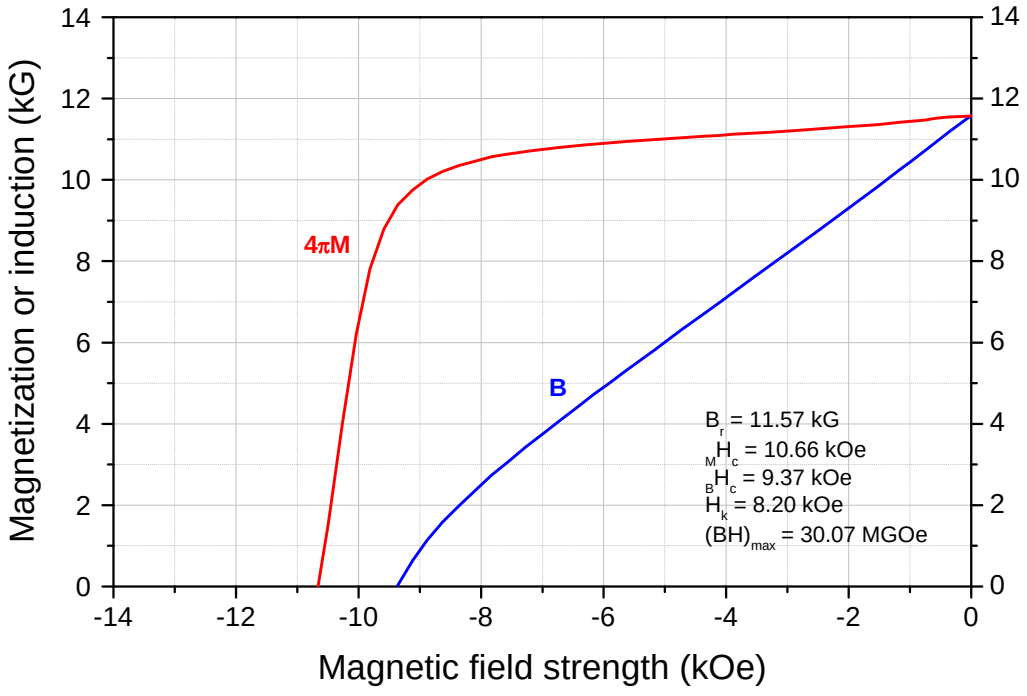

Figure 30. Demagnetization curves of a sintered hybrid $Pr_{17}Fe_{64.75}Co_{10}Al_{0.25}B_8/Pr(Co_{0.8}Fe_{0.2})_5$ (80 wt%/20 wt%) magnet with $(BH)_{max}$ = 30 MGOe.

3.2.7 Does the $Pr(Co,Fe)_5$ component still exist after sintering in sintered hybrid $Pr_2(Fe,Co)_{14}B/Pr(Co,Fe)_5$ magnets?

When using conventional sintering process to synthesize hybrid $Pr_2(Fe,Co)_{14}B/Pr(Co,Fe)_5$ magnets, the green body is heated at 1080°C for 1 hour. Subjecting to such a high temperature for a relatively long time, considerable interdiffusion occurs between the $Pr_2(Fe,Co)_{14}B$ and $Pr(Co,Fe)_5$ components. One may argue that after such a high temperature sintering if the $Pr(Co,Fe)_5$ phase still exists, or the $Pr(Co,Fe)_5$ phase may completely melt into the $Pr_2(Fe,Co)_{14}B$ phase forming a new Pr-rich 2:14:1 phase. If the latter case is true, then the sintered magnets are no longer hybrid magnets and these magnets have basically the same thermal stability as $Pr_2(Fe,Co)_{14}B$ magnets.

In order to have an accurate answer to this important question, we made two types of magnets. The first type of magnets was made by blending $Pr_2(Fe,Co)_{14}B$ and $Pr(Co,Fe)_5$ alloy powders before sintering; the second type of magnets possess the same overall composition as the first type, but prepared using a single alloy.

Figure 31 compares demagnetization curves of these two types of magnets. The composition of type (1) magnet is $Pr_{17}Fe_{66.31}Co_{8.5}Al_{0.19}\ B_8/Pr(Co_{0.8}Fe_{0.2})_{4.664}$ (80 wt%/20 wt%), while the composition of type (2) magnet is $Pr_{17.12}Fe_{57.01}Co_{19.21}Al_{0.15}\ B_{6.51}$. Actually, the overall composition of these two magnets are exactly the same. However, it is obvious from Figure 31 that these two magnets demonstrate quite different demagnetization curves. The type (1) magnet shows higher B_r, higher ${}_MH_c$, and much higher H_k, and $(BH)_{max}$ than those of the type (2) magnet. This result indicates that only partial interdiffusion occurs between the $Pr_2(Fe,Co)_{14}B$ and $Pr(Co,Fe)_5$ components.

It is worth to mention that in sintered hybrid $Pr_2(Fe,Co)_{14}B/Pr(Co,Fe)_5$ magnets the boron content in the $Pr_2(Fe,Co)_{14}B$ component in critical. Because part of the $Pr(Co,Fe)_5$ phase will diffuse into $Pr_2(Fe,Co)_{14}B$ as a result of interdiffusion, if the boron concentration is low, then unfavorable Pr_2Fe_{17} and Pr_2Co_{17} phases will be formed, leading to deteriorate magnetic properties.

3.2.8 Comparison of thermal stability of $Pr_2(Fe,Co)_{14}B$ and hybrid $Pr_2(Fe,Co)_{14}B/Pr(Co,Fe)_5$ based magnets

In order to compare the thermal stability of a hybrid $Pr_2(Fe,Co)_{14}B/Pr(Co,Fe)_5$ based magnet versus a single $Pr_2(Fe,Co)_{14}B$ magnet, two magnet specimens with almost identical magnetic properties were chosen. Demagnetization curves of these two specimens are given in Figure 32. It can be seen from the figure that the induction demagnetization curves (B curves) of these two specimens are completely overlapped, which is critical for a thermal stability experiment. Only under this circumstance can the differences observed be attributed to the differences in intrinsic properties (such as, composition, phase structure and Curie temperate), rather than to differences in structure-sensitive properties (such as coercivity, knee field or linearity of B curve).

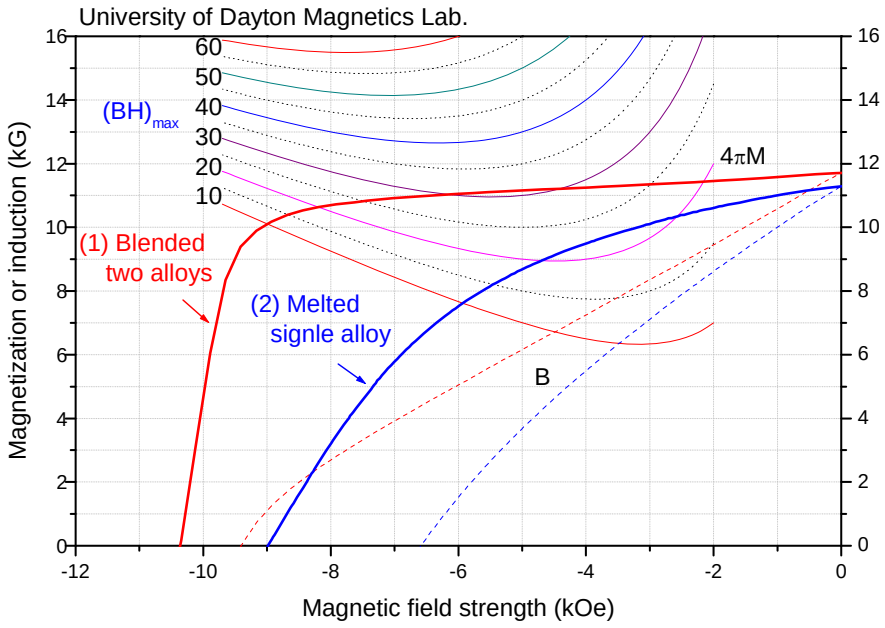

Figure 31. Demagnetization curves of two sintered magnets: (1) magnet prepared by blending $Pr_2(Fe,Co)_{14}B$ and $Pr(Co,Fe)_5$ alloy powders before sintering; (2) magnet has the same overall composition as (1), but prepared using a single alloy.

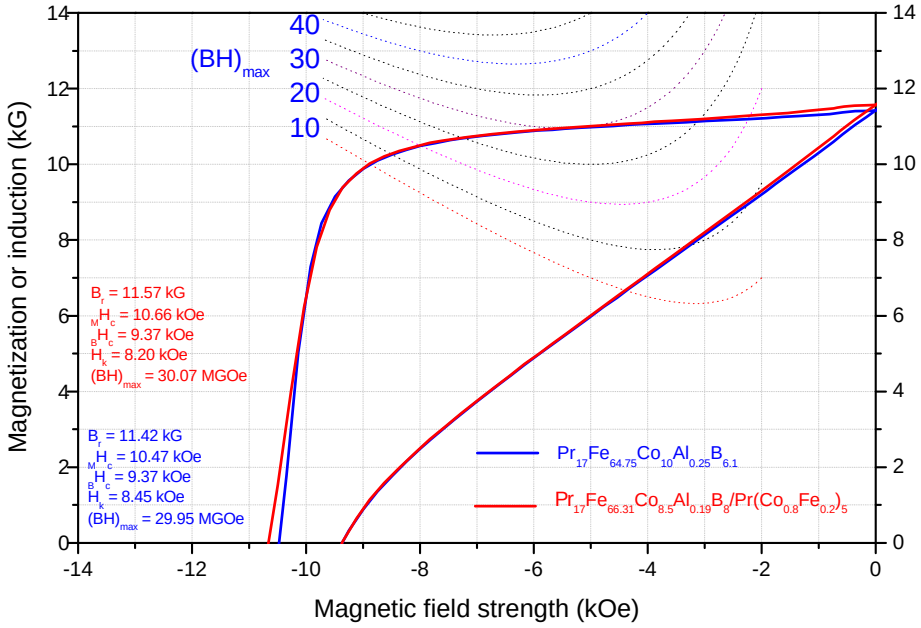

Figure 32. Demagnetization curves of a sintered $Pr_{17}Fe_{64.75}Co_{10}Al_{0.25}B_{6.1}$ magnet and a sintered hybrid $Pr_{17}Fe_{66.31}Co_{8.5}Al_{0.19}B_8/Pr(Co_{0.8}Fe_{0.2})_5$ magnet for thermal stability experiment.

Figure 33 shows the magnetic flux losses versus aging time at 200°C for a pure (non-hybrid) $Pr_2(Fe,Co)_{14}B$ magnet (blue curve) and a sintered hybrid $Pr_2(Fe,Co)_{14}B/Pr(Co,Fe)_5$ magnet (red curve.) It can be seen from Figure 33 that the flux loss of the hybrid magnet is near 20% less than that of the pure $Pr_2(Fe,Co)_{14}B$ magnet. As mentioned previously, these two magnet

specimens have identical magnetic properties, including the same magnitude of $_{M}H_{c}$ and identical induction demagnetization curves. Therefore, any difference of flux losses in the aging process is caused solely by their structure difference. This result serves as another evidence that after sintering at 1080°C for 1 hour, the $Pr(Co,Fe)_5$ phase should still exist in the hybrid magnet. However, the absolute value of the flux losses of the hybrid magnet is still quite high. This problem can be resolved by increasing intrinsic coercivity and obtaining a perfect liner B curve, which will be the focus in the future research.

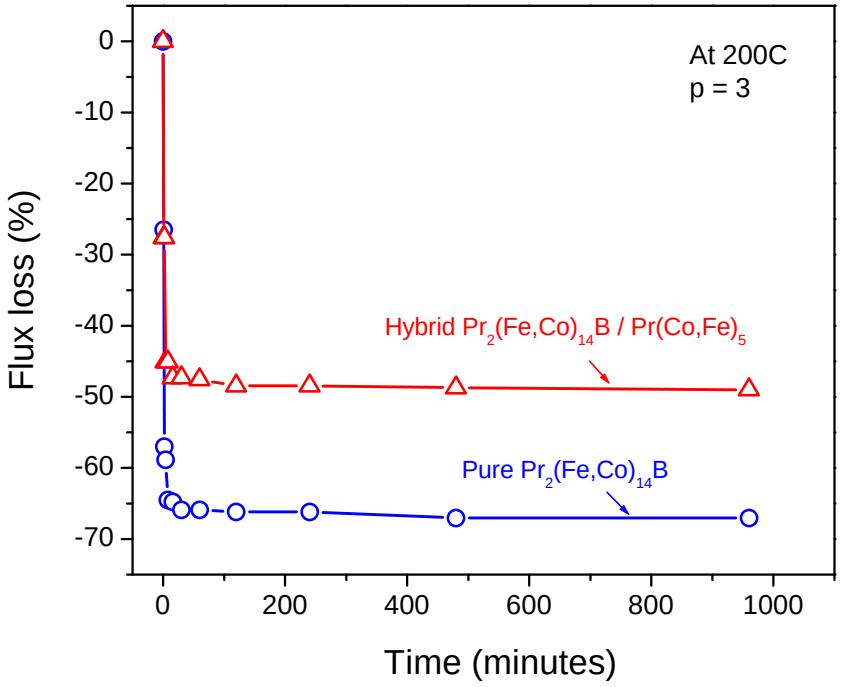

Figure 33. Flux losses in 200°C aging of a sintered hybrid $Pr_2(Fe,Co)_{14}B/Pr(Co,Fe)_5$ magnet and a sintered pure $Pr_2(Fe,Co)_{14}B$ magnet.

3.2.9 Microstructures of sintered hybrid $Pr_{17}Fe_{68.21}Co_{8.5}Al_{0.19}B_{6.1}/Pr(Co_{0.8}Fe_{0.2})_5$ magnets

Microstructures of sintered hybrid $Pr_{17}Fe_{68.21}Co_{8.5}Al_{0.19}B_{6.1}/Pr(Co_{0.8}Fe_{0.2})_5$ were observed using SEM and the phases were analyzed by SEM-EDS. Figures 34 (a – c) illustrate SEM backscattered electron images of a $Pr_{17}Fe_{68.21}Co_{8.5}Al_{0.19}B_{6.1}/Pr(Co_{0.8}Fe_{0.2})_5$ magnet under different magnifications. Basically, three different phases were observed: a dark-grey phase (A), a white phase (B), and a ligh-grey phase (C). The average grain size for the A phase is approximately 10 micrometers.

Figure 35 shows results of SEM-EDS analyses. According to these results, the dark grey A phase is a $Pr_2(Fe,Co)_{14}B$, the light grey B phase is a Pr-rich phase, and the light grey C phase seems to be a $Pr(Co,Fe)_2$ phase. It can also be seen from Figures 35 (B) and (C) that both the B and C phase have a repetatively high oxygen concentration. Processing should be improved to minimize oxygen in future experiments.

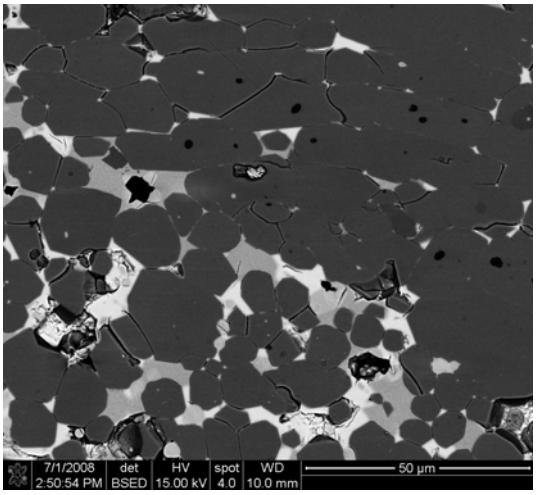

(a)

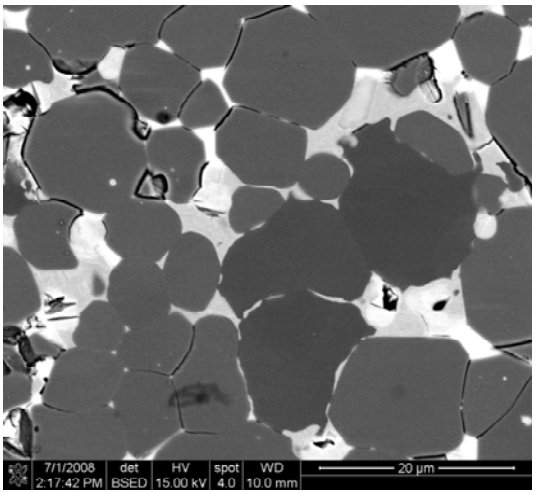

(b)

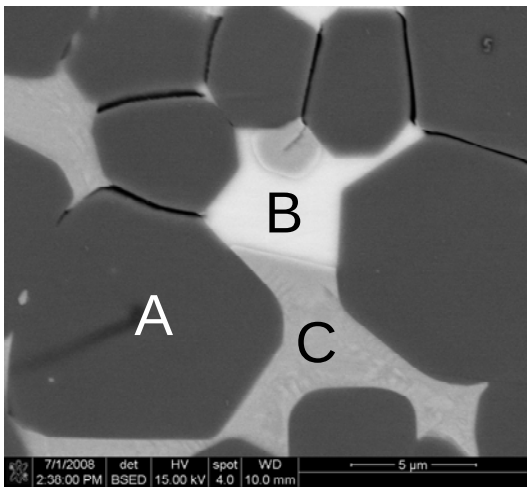

(c)

Fig. 34. SEM back-scatterd electron images of a sintered hybrid $Pr_{17}Fe_{68.21}Co_{8.5}Al_{0.19}B_{6.1}$/ $Pr(Co_{0.8}Fe_{0.2})_5$ (80 wt%/20 wt%) magnet under different magnification.

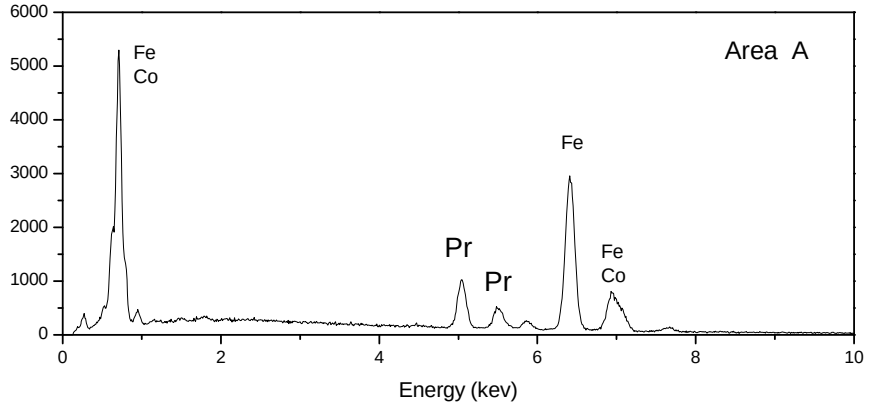

(A)

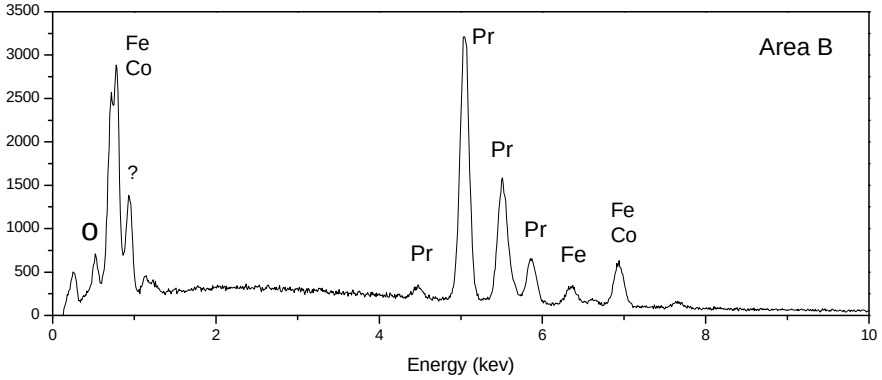

(B)

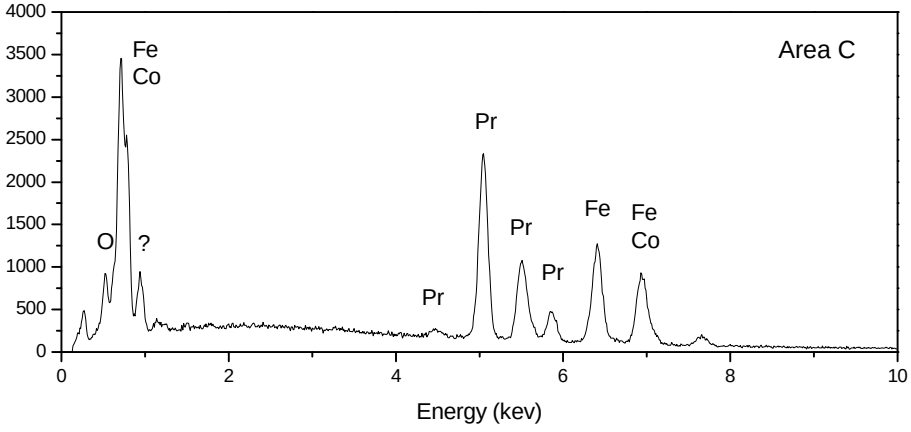

(C)

Fig. 35. Results of SEM-EDS analyses for a sintered hybrid $Pr_{17}Fe_{68.21}Co_{8.5}Al_{0.19}B_{6.1}$/ $Pr(Co_{0.8}Fe_{0.2})_5$ (80 wt%/20 wt%) magnet.

3.3 $Pr_2(Fe,Co)_{14}B/Pr(Co,Fe)_5$ Hybrid Magnets Synthesized Using Induction Sintering Process

When using conventional sintering process, considerable interdiffusion occurs, resulting in decreased volume of the 1:5 component. In order to minimize the interdiffusion between the $Pr_2(Fe,Co)_{14}B$ and $Pr(Co,Fe)_5$ components, the sintering temperature must be lowered and/or the sintering time must be shortened. For these purpose, we tried to use the induction sintering instead of conventional sintering.

The induction sintering was performed in our hot press furnace and the sintering temperatures used were 1000 - 1080°C and the sintering time was 15 or 30 minutes. Table 4 lists magnetic properties and density values of $Pr_2(Fe,Co)_{14}B$ magnets prepared using induction sintering. Table 5 lists magnetic properties and density values of hybrid $Pr_{17}Fe_{66.31}Co_{8.5}Al_{0.19}$ B_8/ $Pr(Co_{0.8}Fe_{0.2})_{4.664}$ magnets. It can be seen from these tables that magnets prepared using induction sintering have relatively low ${}_MH_c$ as compared with magnets made using conventional sintering.

Figure 36 shows the effect of increasing the temperature of induction sintering from 1000 to 1080°C. Figure 37 summarizes the effect of increasing the temperature of induction sintering on magnetic properties and density of hybrid $Pr_{17}Fe_{66.31}Co_{8.5}Al_{0.19}$ B_8/$Pr(Co_{0.8}Fe_{0.2})_{4.664}$ (80 wt%/ 20 wt%) magnets.

It is well known that the post-sintering heat treatment effectively enhances ${}_MH_c$ of sintered $Nd_2Fe_{14}B$ based permanent magnets. We investigated its effect of post-sintering heat treatment on magnetic properties of hybrid $Pr_2(Fe,Co)_{14}B$/ $Pr(Co,Fe)_5$ magnets prepared using induction sintering and the results are given in Table 6. In Table 6, suffix "H" denotes specimens subjected to a post-sintering at 580°C for 20 minutes.

As shown in Table 6, the effect of the post-sintering heat treatment on enhancing is limited. We only observed a near 2 MGOe increase of $(BH)_{max}$ in Specimen 96H, and demagnetization curves of 96H and 96 are shown in Figure 38.

Table 4. Magnetic Properties of $Pr_2(Fe,Co)_{14}B$ Magnets Synthesized Using Induction Sintering

ID	Composition	Sintering temp/ time (°C/min.)	B_r (kG)	${}_MH_c$ (kOe)	H_k (kOe)	$(BH)_{max}$ (MGOe)	Density (g/cm^3)
91	$Pr_{17}Fe_{64.75}Co_{10}Al_{0.25}$ B_8	1030 / 30	11.27	6.31	5.4	28.01	7.31
92	$Pr_{17}Fe_{64.75}Co_{10}Al_{0.25}$ B_8	1080 / 30	11.57	4.31	3.81	25.89	7.45
93	$Pr_{17}Fe_{66.31}Co_{8.5}Al_{0.19}$ B_8	1030 / 30	11.09	7.31	6.19	27.41	7.07
96	$Pr_{17}Fe_{66.31}Co_{8.5}Al_{0.19}$ B_8	1030 / 30	11.38	6.99	5.05	26.81	7.27
97	$Pr_{17}Fe_{66.31}Co_{8.5}Al_{0.19}$ B_8	1030 / 15	11.41	6.96	5.06	26.92	7.26
102	$Pr_{17}Fe_{66.31}Co_{8.5}Al_{0.19}$ B_8	1080 / 15	11.17	5.73	3.96	24.16	7.3
104	$Pr_{17}Fe_{64.75}Co_{10}Al_{0.25}$ B_8	1080 / 15	11.37	4.88	3.95	25.1	7.27

Table 5. Magnetic Properties of $Pr_2(Fe,Co)_{14}B/Pr(Co,Fe)_5$ (80 wt%/20 wt%) Magnets Synthesized Using Induction Sintering

ID	Sintering temp / time (°C/min.)	B_r (kG)	$_MH_c$ (kOe)	H_k (kOe)	$(BH)_{max}$ (MGOe)	Density (g/cm^3)
100	1000 / 15	9.37	4.15	2	13.77	6.19
95	1030 / 15	11.08	4.32	3.04	21.13	7.12
98	1030 / 15	10.59	3.87	2.75	18.66	7.12
103	1080 / 15	10.95	4.09	2.84	19.94	7.17

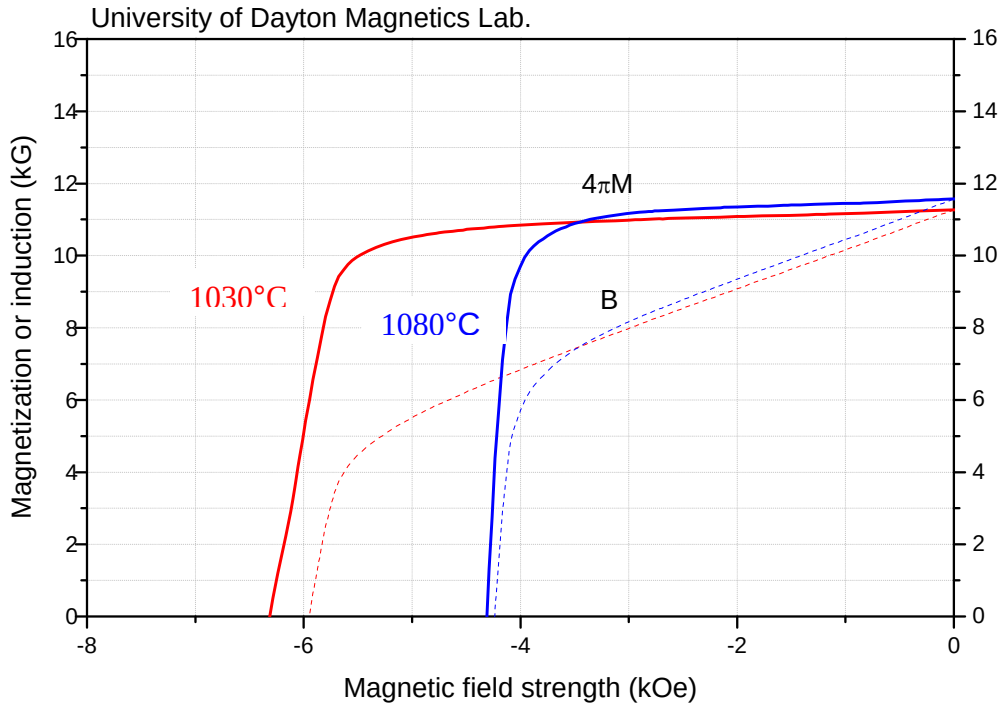

Figure 36. Demagnetization curves of $Pr_{17}Fe_{64.75}Co_{10}Al_{0.25}$ B_8 magnets induction sintered at 1030 and 1080°C, respectively.

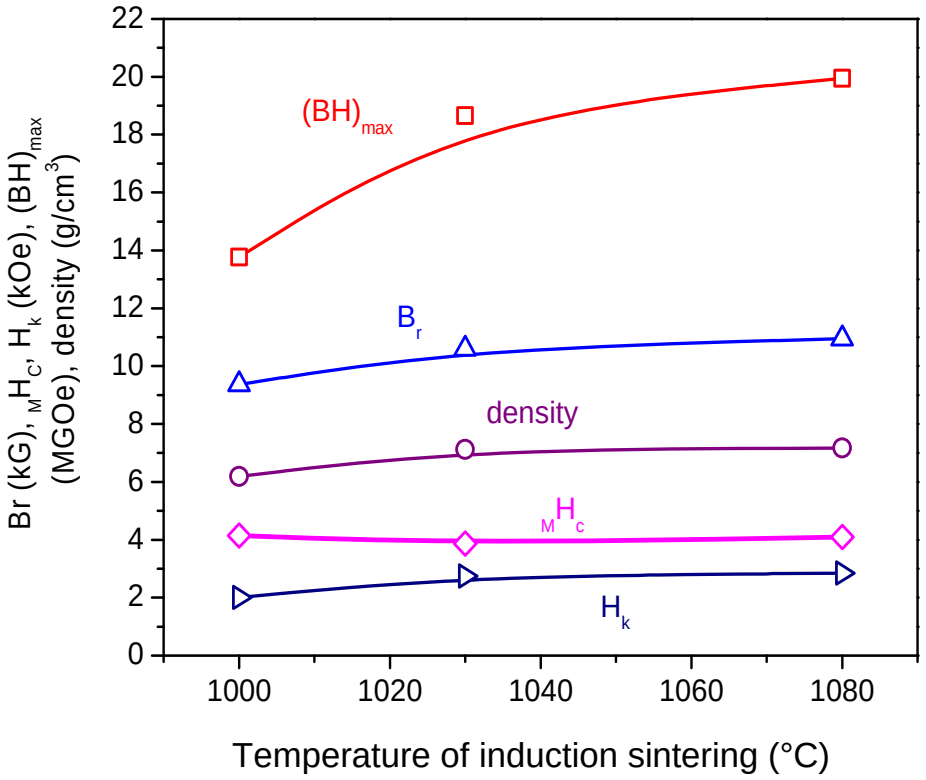

Figure 37. Effect of the temperature of induction sintering on magnetic properties and density of $Pr_{17}Fe_{66.31}Co_{8.5}Al_{0.19}$ B_8/$Pr(Co_{0.8}Fe_{0.2})_{4.664}$ (80 wt%/20 wt%) magnets.

Table 6. Effect of Post-sintering Heat Treatment

ID	Composition	B_r (kG)	$_MH_c$ (kOe)	H_k (kOe)	$(BH)_{max}$ (MGOe)	Density (g/cm^3)
91	$Pr_{17}Fe_{64.75}Co_{10}Al_{0.25}$ B_8	11.27	6.31	5.4	28.01	7.31
91H	$Pr_{17}Fe_{64.75}Co_{10}Al_{0.25}$ B_8	11.24	6.24	5.36	27.82	
93	$Pr_{17}Fe_{66.31}Co_{8.5}Al_{0.19}$ B_8	11.09	7.31	6.19	27.41	7.07
93H	$Pr_{17}Fe_{66.31}Co_{8.5}Al_{0.19}$ B_8	11.14	7.42	6.2	27.57	
96	$Pr_{17}Fe_{66.31}Co_{8.5}Al_{0.19}$ B_8	11.38	6.99	5.05	26.81	7.27
96H	$Pr_{17}Fe_{66.31}Co_{8.5}Al_{0.19}$ B_8	11.53	7.34	5.6	28.46	
95	$Pr_{17}Fe_{66.31}Co_{8.5}Al_{0.19}$ B_8/ $Pr(Co_{0.8}Fe_{0.2})_{4.664}$ (80 wt%/20 wt%)	11.08	4.32	3.04	21.13	7.12
95H	$Pr_{17}Fe_{66.31}Co_{8.5}Al_{0.19}$ B_8/ $Pr(Co_{0.8}Fe_{0.2})_{4.664}$ (80 wt%/20 wt%)	11.12	4.65	3	21.18	

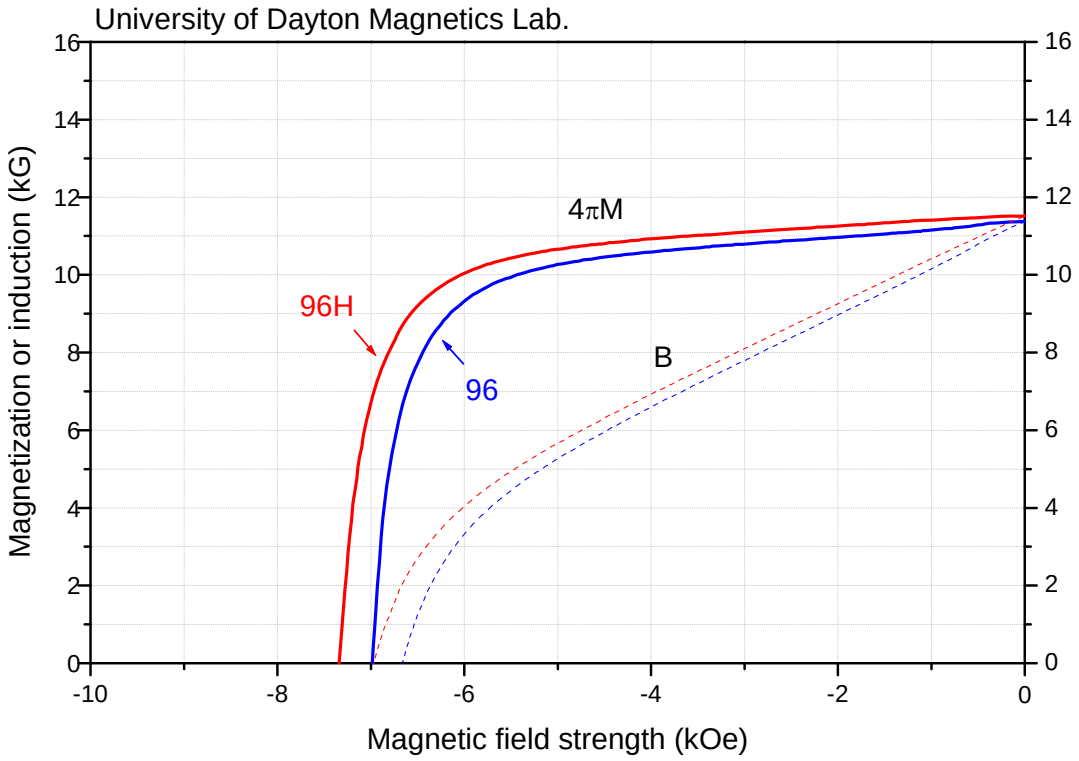

Figure 38. Demagnetization curves of an induction sintered specimen (96) and the same specimen after subjecting post sintering heat treatment at 580°C for 20 minutes (96H).

3.4 Explore Possibility of Synthesizing $Pr_2(Fe,Co)_{14}B/Pr(Co,Fe)_5$ Hybrid Magnets Using Nanoparticle Approach

Magnetically hard nanoparticles have attracted great interest because of their potential applications, including the development of high performance nanocomposite magnets. Recently, a technique using high energy ball milling with surfactant assistance was reported to prepare nanoparticles such as $SmCo_5$, Sm_2Co_{17}, $Nd_2Fe_{14}B$, and $PrCo_5$ [7 -11]. We believe that compacting this type of powder and forming a desired bulk magnet will be the next challenging goal. In this work, we synthesized $PrCo_5$ nanopowders by surfactant-assisted ball milling and further made an effort to fabricate $PrCo_5$ bulks by using the hot compaction process.

$PrCo_5$ alloy was prepared by arc melting in argon using pure metals, with calculated composition $Pr_{18}Co_{82}$ to compensate the Pr loss during process. The alloy was then crushed and grinded down to less than 250 μm as the starting powder. The powder was milled in a vial with carbon-steel balls using a Spex 8000M high energy mill. The weight ratio of the balls to the powders is 10:1. Heptane (99.9%) was used as the solvent and oleic acid (90%) was used as the surfactant in the wet milling. The amount of solvent and surfactant used was 55% and 10% of the weight of the starting powders, respectively. After 4 hours of milling, the resultant $PrCo_5$ slurry was washed by heptane and dried in vacuum. The dried powders loaded in a die were heated to the compaction temperature (200~525°C) in vacuum and meanwhile compacted under a pressure of ~1.7 x 10^8 Pa. The obtained $PrCo_5$ bulks were rod shaped, approximately 8 mm in diameter and ~8-10 mm in length.

Powder samples for magnetic characterization were prepared by mixing the nanoparticles with epoxy inside a glove box and letting it cure in the magnetic field to obtain an aligned sample. A KJS hysteresisgraph and vibrating sample magnetometer (VSM) were used in magnetic measurements. Structural and morphology characterizations were made using x-ray diffraction (XRD), a transmission electron microscopy (TEM), a scanning electron microscope (SEM), and energy dispersive spectroscopy (EDS) analyses. Powder samples for TEM were prepared by dispersing the as-milled $PrCo_5$ slurry into heptane with ultrasonically vibrating and drying on carbon coated copper grids.

Figures 39 and 40 show TEM and SEM images of the particles after 4 hours of milling. During preparation of the powder samples, some powder particles were suspended in the solvent after ultrasonic vibration, which have a particle size of 20 nm or less as indicated by the TEM image in Figure 39. Meanwhile, the other particles sedimentated gradually, and the SEM image revealed that these flake-shaped particle sizes are smaller than ~400 nm in thickness and 5 μm in length as shown in Figure 40. One flake may be an agglomerate of the nanoparticles or one polycrystalline particle. Thus, $PrCo_5$ powders after 4 hours of milling consist of round-shape nanoparticles and flake-shaped particles. SEM/EDS analysis on the milled powder is shown in Figure 41 (a). It is obvious that there is no Fe in the milled powder, thus Fe contamination didn't happen during this milling process.

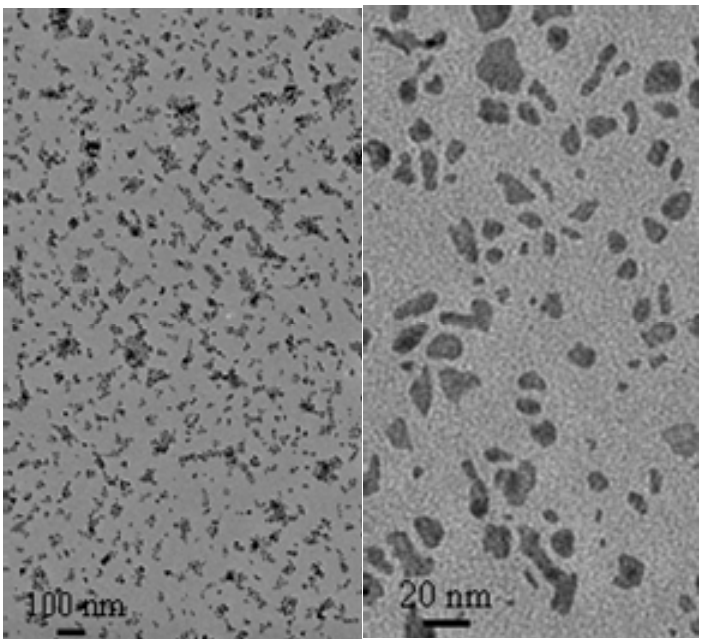

Figure 39. TEM images of the particles suspended in the solvent.

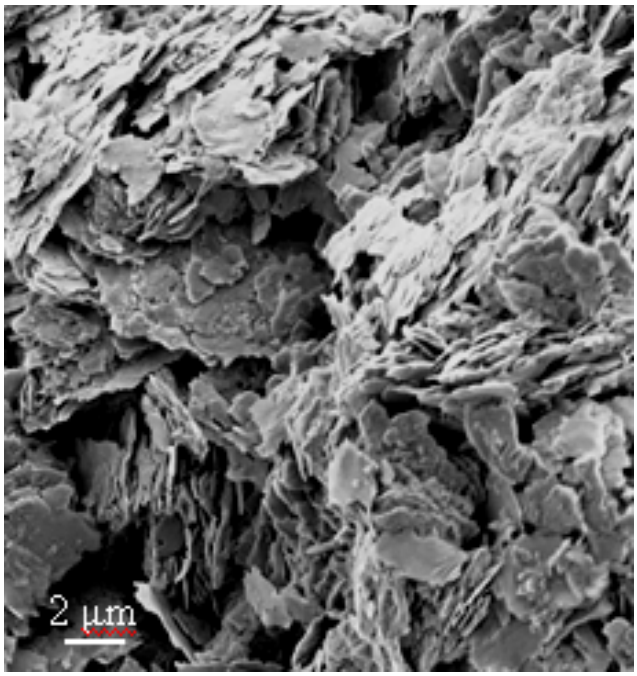

Figure 40. SEM image of the particles sedimentated the bottom of the solvent.

The test result of VSM sample is shown in Figure 42. The M-H curves indicate $B_r(x)/B_r(z)$ ratio of ~ 0.6 and intrinsic coercivity of 6.67 kOe, demonstrating an anisotropic behavior. Here, $B_r(x)$ and $B_r(z)$ present the remanance of perpendicular and parallel to the aligned direction, respectively.

After reducing the surfactant content, the nanopowder was successfully compacted to bulk samples. A bulk sample pressed at 200˚C revealed almost the same XRD patterns as the milled powder shown in Figure 43. The diffraction peaks of the starting powder show a small amount of Pr_5Co_{19} phase in addition to the main phase $PrCo_5$. The broadening peaks for both as-milled powder and the bulk reveal fairly small crystallite size. As seen in Figure 44, the SEM image of the bulk shows several flake particles fused together as a “cluster”, which may consist of multi-nanograins. This cluster type structure matches the morphology of the milled powders as described earlier. The evidence above indicates the compaction at 200˚C did not change the crystalline structure of the particles. The intrinsic coercivity of the bulk sample pressed at 200˚C was slightly reduced to 5.22 kOe seen in Figure 45. Figure 41 shows the oxygen in the bulk is slightly higher than that in the powder, which may result in the coercivity of the bulk being lower than that of the powder.

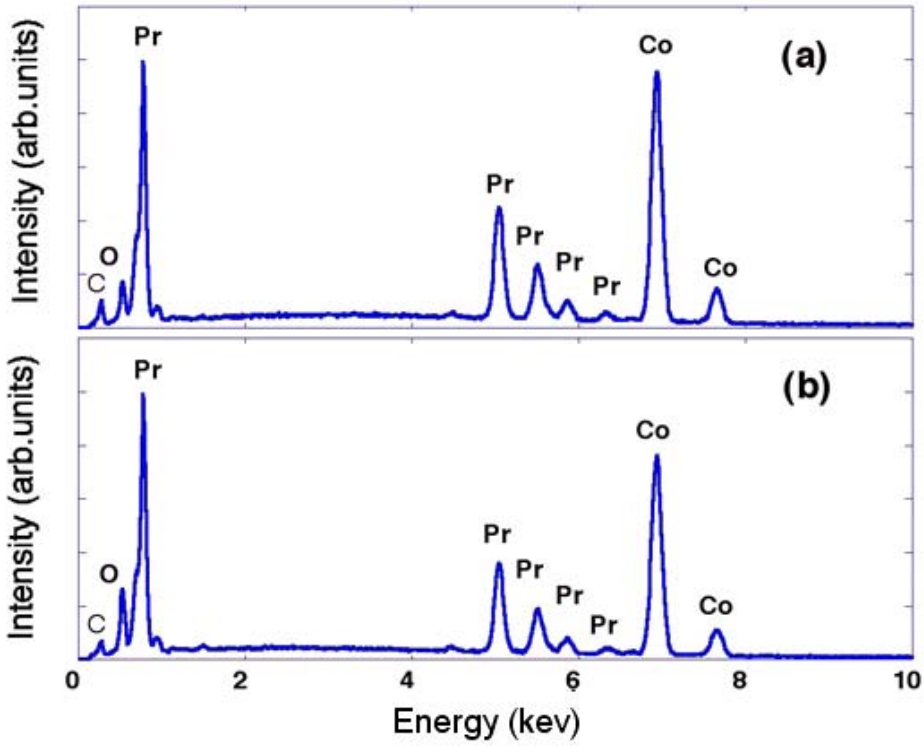

Figure 41. SEM/EDS results for the PrCo5 powder and bulk:
(a) Powder milled 4 h; (b) Bulk pressed at 200°C.

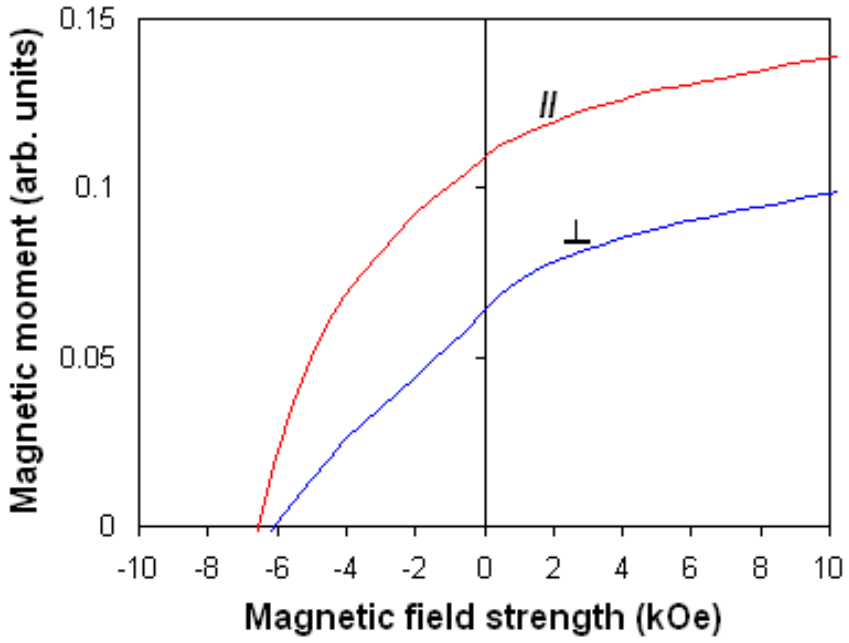

Figure 42. Magnetization curves of 4h milling $PrCo_5$ powder epoxy sample by VSM.

The bulk pressed at 200˚C has density of 6.26 g/cm^3. As the pressing temperature increases from 200˚C to 300, 400 and 525˚C, the bulk becomes denser, as shown in Figure 45. The highest density is 7.70 g/cm^3, 92% of theoretical density; however, the coercivity decreases as the temperature increases. XRD analysis for the bulk magnets pressed at 400 and 525˚C shows the existence of PrO_2 and cobalt, which indicates some oxidation of $PrCo_5$ occurred during the process. Since the grain growth is not significant at temperatures below 525°C through observing the SEM microstructure, the decrease in coercivity is mainly related to the loss of praseodymium from $PrCo_5$ and the appearance of the soft magnetic cobalt phase. In this pressing process, the oxygen likely came from two sources, one from the residual oxygen in the vacuum chamber and another from the residual oleic acid of powders. The as-milled powder was washed three times in heptane, and most of the surfactant oleic acid was likely dissolved into heptane. But it is difficult to totally remove oleic acid absorbed on the particle surface. Further investigation on the effect of surfactant on the compaction process and the bulk properties is underway.

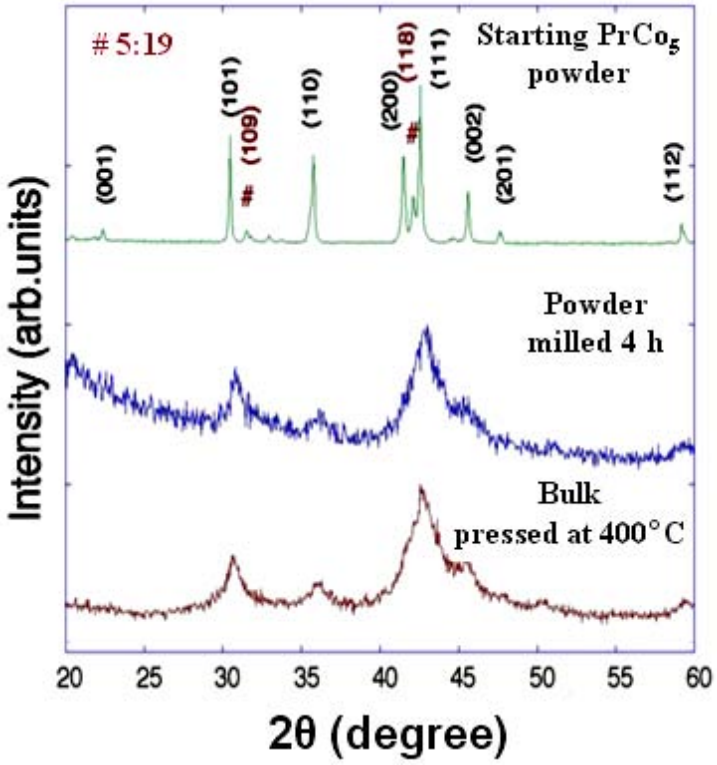

Figure 43. XRD patterns for $PrCo_5$ starting powder, milled 4 h powder, and bulk pressed at 200˚C.

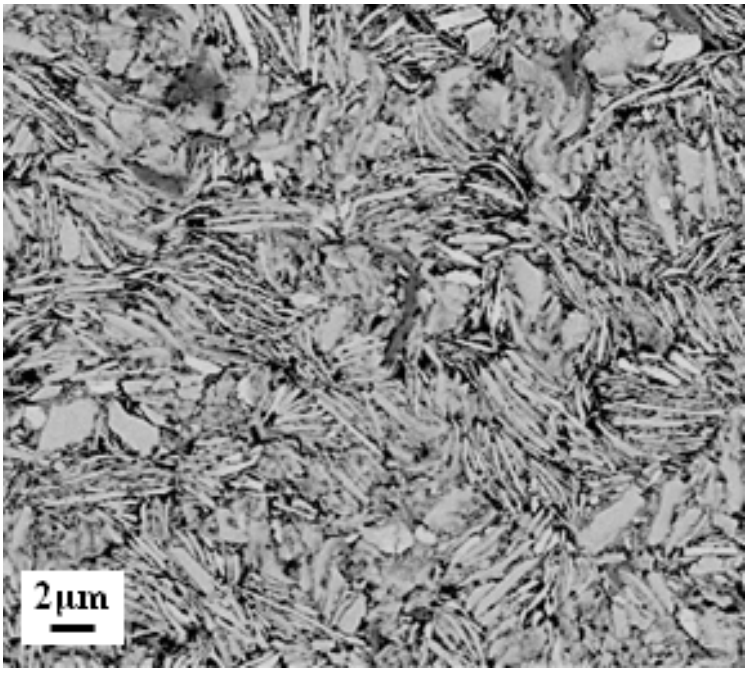

Figure 44. SEM image of $PrCo_5$ bulk compacted at 200˚C.

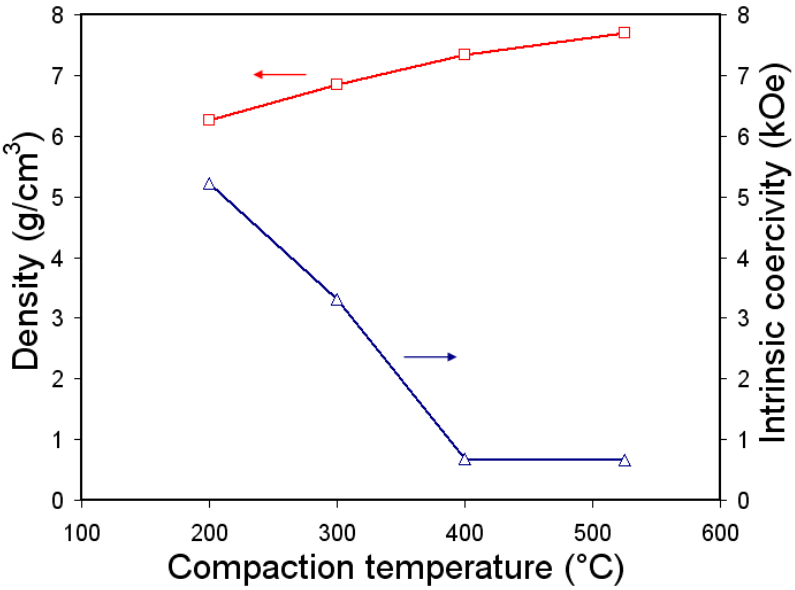

Figure 45. Effect of pressing temperature on the coercivity and density of $PrCo_5$ bulk specimens.

In this experiment, $PrCo_5$ nanopowder was produced by surfactant-assisted high energy ball milling. The powders consist of round-shape nanoparticles and flake-shaped particles. The intrinsic coercivity of the powders milled 4 hours is 6.7 kOe. Using the nanopowders, $PrCo_5$ bulk magnets have been successfully fabricated by compaction at 200~525°C. The bulk magnet has cluster microstructure with nanocrystaline. It is found that the density of the bulk increases with the compaction temperature. The density of the bulk up to 92% theoretical value has been obtained. The coercivity of the bulk decreases as the compaction temperature increasing because of oxidation during process.

4. CONCLUSIONS

Hybrid $Pr_2(Fe,Co)_{14}B/Pr(Co,Fe)_5$ magnets with nanograin and micrograin structures were studied and synthesized in this project using various approaches, including rapid hot press and hot deformation process, conventional sintering process, and rapid induction sintering process. The possibility of applying nanoparticles to synthesize bulk magnets was also explored.

The magnetic property of $(BH)_{max}$ = 36.9 MGOe was obtained in a hybrid $Pr_{14.1}Fe_{73.3}Co_{5.1}Ga_{0.5}B_{7.1}/Pr(Co_{0.8}Fe_{0.2})_5$ magnet containing 10 wt% $Pr(Co,Fe)_5$ component which will give much better thermal stability compared to the commercial available magnets with the same $(BH)_{max}$.. In hybrid $Pr_2(Fe,Co)_{14}B/ Pr(Co,Fe)_5$ magnets containing 20 wt% $Pr(Co,Fe)_5$, $(BH)_{max}$ = 33.2 MGOe was obtained. These magnetic properties were obtained in hybrid nanograin magnets prepared using rapid hot press and hot deformation.

Hybrid magnets synthesized using sintering process showed relatively low intrinsic coercivity values. The best $(BH)_{max}$ obtained was 30.07 MGOe. The boron content in the $Pr_2(Fe,Co)_{14}B$ component strongly affects the magnetic performance of sintered hybrid $Pr_2(Fe,Co)_{14}B/ Pr(Co,Fe)_5$ magnets. When the boron content was increased from 6.1% to 8%, the increase of B_r, $_MH_c$, H_k, and $(BH)_{max}$ was 0.62%, 32.5%, 126.5%, and 21.7%, respectively. In a long-term aging experiment performed at 200°C, the flux losses of a sintered hybrid $Pr_2(Fe,Co)_{14}B/ Pr(Co,Fe)_5$ magnet demonstrated near 20% less than that of a sintered pure $Pr_2(Fe,Co)_{14}B$ magnet.

In addition, $PrCo_5$ nanopowder was produced by surfactant-assisted high-energy ball milling. The intrinsic coercivity of the powders milled 4 hours reached 6.7 kOe. Using the nanopowders, $PrCo_5$ bulk magnets were successfully fabricated by compaction at 200~525°C. The bulk magnet has cluster microstructure with nanocrystalline. The density of the bulk up to 92% theoretical value was obtained.

5. BIBLIOGRAPHY

[1] M. Sagawa, S. Fujimura, N. Togawa, H. Yamamoto, and Y. Matruura, "New material for permanent magnets on a base of Nd and Fe," *J. Appl. Phys*. 55 (1984), 2083.

[2] M. Sagawa, S. Fujimura, H. Yamamoto, and Y. Matruura, and K. Hiraga, "Permanent magnet materials based on the rare earth-iron-boron tetragonal compounds," *IEEE Trans. Magn*. 20 (1984), 1584.

[3] M. Zhang, D. Ma, X. Jiang, and S. Liu, "Effects of additive elements on magnetic properties of sintered Nd-B-Fe magnet," *Proc. 8th Int'l. Workshop on REM*, Ed. K.J. Strnat (1985), 541.

[4] S. Liu, "Effect of Nanograin Structure on Magnetic Properties of Rare Earth Permanent Magnets," *Proc. 18th Workshop on HPM*, Vol. 2 (2004), 690.

[5] S. Liu, B. Cui, S. Bauser, R. Leese, J.S. Hilton, R.H. Yu, A. Kramp, J. Dent, and D. Miles, "Approach to synthesizing bulk, fully dense anisotropic nanocomposite rare earth permanent magnets," *Proc. 17th Int'l. Workshop on REM*, Ed. G.C. Hadjipanayis and M.J. Bonder, (2002), 939.

[6] Lee, D., Bauser, S., Higgins, A., Chen, C., Liu, S., Huang, M.Q., Peng, Y.G., and Laughlin, D.E., "Bulk Anisotropic Composite Rare Earth Magnets," *J. Appl. Phys.*, 99 (2006), 08B516.

[7] V. M. Chakka, B. Altuncevahir, Z. Q. Jin, Y. Li, and J. P. Liu, "Magnetic nanoparticles produced by surfactant-assisted ball milling," *J. Appl. Phys.* 99(2006), 08E912.

[8] Y. Wang, Y. Li, C. Rong, and J. P. Liu, "Sm-Co hard magnetic nanoparticles prepared by surfactant-assisted ball milling," Nanotechnology 18 (2007), 465701.

[9] M. Yue, Y. Wang, N. Poudyal, C. Rong, and J. P. Liu, "Preparation of Nd-Fe-B nanoparticles by surfactant-assisted ball milling technique," *J. Appl. Phys.* 105 (2009), 07A708.

[10] N.G. Akdogan, G. C. Hadjipanayis, and D. J. Sellmyer, "Anisotropic Sm-(Co,Fe) nanoparticles by surfactant-assisted ball milling," *J. Appl. Phys.* 105 (2009), 07A710.

[11] N.G. Akdogan, G. C. Hadjipanayis, and D. J. Sellmyer, "Anisotropic $PrCo_5$ nanoparticles by surfactant-assisted ball milling," EG-07 presented at *INTERMAG 2009*, CA, USA.